



**Breakdown Mechanisms of Preformed Al_2O_3 , Cr_2O_3
and SiO_2 Scales in $\text{H}_2/\text{H}_2\text{O}/\text{H}_2\text{S}$ Environments at 950°C**

June 1, 1988

Report Prepared by

G. M. Kim and G. H. Meier

Department of Materials Science and Engineering
University of Pittsburgh
Pittsburgh, PA 15261

under

Subcontract Number 19X-43346-C

Program Manager: R. R. Judkins

for

OAK RIDGE NATIONAL LABORATORY
Oak Ridge, Tennessee 37831
operated by
MARTIN MARIETTA ENERGY SYSTEMS, INC.
for the
U.S. DEPARTMENT OF ENERGY
under Contract No. DE-AC05-84OR21400

OAK RIDGE NATIONAL LABORATORY

CENTRAL RESEARCH LIBRARY

CIRCULATION SECTION

4500N ROOM 175

LIBRARY LOAN COPY

DO NOT TRANSFER TO ANOTHER PERSON

If you wish someone else to see this
report, send in name with report and
the library will arrange a loan.

Printed in the United States of America. Available from
National Technical Information Service
U.S. Department of Commerce
5285 Port Royal Road, Springfield, Virginia 22161
NTIS price codes - Printed Copy: A04 Microfiche A01

This report was prepared as an account of work sponsored by an agency of the United States Government. Neither the United States Government nor any agency thereof, nor any of their employees, makes any warranty, express or implied, or assumes any legal liability or responsibility for the accuracy, completeness, or usefulness of any information, apparatus, product, or process disclosed, or represents that its use would not infringe privately owned rights. Reference herein to any specific commercial product, process, or service by trade name, trademark, manufacturer, or otherwise, does not necessarily constitute or imply its endorsement, recommendation, or favoring by the United States Government or any agency thereof. The views and opinions of authors expressed herein do not necessarily state or reflect those of the United States Government or any agency thereof.

Breakdown Mechanisms of Preformed Al_2O_3 , Cr_2O_3
and SiO_2 Scales in $\text{H}_2/\text{H}_2\text{O}/\text{H}_2\text{S}$ Environments at 950°C

June 1, 1988

Research sponsored by the U.S. Department of Energy,
Advanced Research and Technology Development
Fossil Energy Materials Program

Report Prepared by

G. M. Kim and G. H. Meier

Department of Materials Science and Engineering
University of Pittsburgh
Pittsburgh, PA 15261

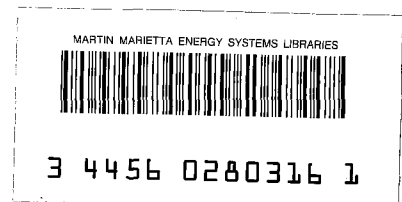
under

Subcontract Number 19X-43346-C

Program Manager: R. R. Judkins

for

OAK RIDGE NATIONAL LABORATORY
Oak Ridge, Tennessee 37831
operated by
MARTIN MARIETTA ENERGY SYSTEMS, INC.
for the
U.S. DEPARTMENT OF ENERGY
under Contract No. DE-AC05-84OR21400



Breakdown Mechanisms of Preformed Al_2O_3 , Cr_2O_3
and SiO_2 Scales in $\text{H}_2/\text{H}_2\text{O}/\text{H}_2\text{S}$ Environments at 950°C

Gil M. Kim and Gerald H. Meier

ABSTRACT

The breakdown mechanisms of preformed oxide scales, Cr_2O_3 , Al_2O_3 and SiO_2 , have been studied at 950°C at low oxygen and high sulfur potentials.

For Cr_2O_3 on Ni-30Cr, sulfur penetration occurs through thin areas in the Cr_2O_3 scale. These thinner areas were formed over voids formed during preoxidation because the voids act as chromium diffusion barriers. Internal sulfides form at the rim of the voids where the chromium activity is high. The filling of voids by the sulfides and the progressive formation of sulfides through the scale establish sulfide rich channels which are easy paths for cation transport. The breakdown occurs once the channels are introduced.

For Al_2O_3 on Fe-18Cr-6Al-1Hf, sulfur reacts with metallic iron on the surface and HfO_2 extending through the Al_2O_3 scale to form iron sulfides and hafnium rich sulfides, respectively. These sulfides provide easy paths for inward diffusion of sulfur ions and outward diffusion of base metal ions to form internal sulfides at the craters around Hf rich phases, and external sulfides at the scale/gas interface, respectively.

For SiO_2 on Ni-20Si, although porosity can form at the scale/gas interface due to the high vapor pressures of SiS and SiO , the formation of a thin layer of vitreous silica and good scale adherence provide better resistance to sulfur penetration than do Cr_2O_3 and Al_2O_3 .

Key Words: Fe-18Cr-6Al-1Hf, Ni-20Si, Ni-30Cr, Scale Breakdown, Sulfidation/Oxidation

INTRODUCTION

Current high temperature alloys and coatings are designed to resist high temperature degradation in highly oxidizing atmospheres by the formation of a protective oxide film (usually Cr_2O_3 , Al_2O_3 , or SiO_2) by selective oxidation. However, in some processes (e.g. coal gasification) the alloys and coatings are exposed to environments with low oxygen potentials and high potentials of other reactants such as sulfur and carbon.^{1,2} Exposure to such environments often leads to formation of reaction products, such as sulfides or carbides, which are less protective than oxides even in atmospheres where Cr_2O_3 , Al_2O_3 , or SiO_2 are thermodynamically stable. Preformed films of Cr_2O_3 , Al_2O_3 or SiO_2 should continue to grow in these atmospheres and improve corrosion resistance until the scales break down due to the formation of less protective reaction products. The length of time a given oxide remains protective is expected to depend on its thickness and integrity, the composition of the underlying alloy, the atmosphere composition, and temperature.³

The objective of this research is directed toward studying the mechanisms by which preformed oxide layers are degraded in high P_{S_2} and low P_{O_2} environments.

"Research sponsored by the U.S. Department of Energy, AR&TD
Fossil Energy Materials Program, DOE/FE AA 15 10 10 0, Work
Breakdown Structure Element PITT-3"

BACKGROUND

If alloys and metallic coatings are exposed to low oxygen and high sulfur potentials, the scales will be composed of both oxides and sulfides although the kinetics and morphology of the scale depend on the initial exposure conditions. Yurek, et al⁴ studied the effects of $H_2/H_2S/H_2O$ gas mixtures on pure chromium and Fe-Cr alloys. They concluded that the amount of sulfide formed increased as the H_2O/H_2S ratio decreased. If the rate of supply of oxygen is much higher than the rate of sulfur, Cr_2O_3 is stable. Eventually sulfur penetrates the Cr_2O_3 scale by solid state diffusion or gas phase diffusion through defects.

Degradation resistance in sulfur bearing gases can be improved by the preformation of an oxide scale on an alloy surface prior to exposure to such environments, but eventually the oxide scale will be broken down. Such degradation of an alloy can occur by the diffusion of base metal cations such as Ni and Fe through the oxide scale to the scale/gas interface and subsequently by sulfidation of these elements, or by the diffusion of sulfur through the oxide scale to the substrate and internal sulfidation at the scale/alloy interface. Since Bruce and Hancock⁵ proposed that the oxide scales continuously develop and heal mechanical defects, Rahmel⁶ showed the formation of sulfides along the edges and the corners of specimens, indicating that mechanical breakdown of the scale is responsible for the sulfur attack and formation of sulfides beneath the scale.

It has been suggested⁷ that sulfur-bearing species penetrate the oxide scale through the oxide grain boundaries and react with cations such as Cr and Al to form internal sulfides at or near the scale/alloy interface. Progressive formation of sulfides at the sulfide/oxide interface, by the reaction between outward moving metal ions and inward moving sulfur-bearing species, provide sulfide-rich channels through the scale which are easy paths for metal ion transport. This enables base

metal sulfides to form at the scale/gas interface. In the case of the diffusion of sulfur-bearing gases through cracks or pores in preformed Cr_2O_3 , the sizes of defects determine whether sulfide can form in or beneath the scale adjacent to the defects.⁸ When the physical defects are very narrow, the local oxygen potential in the gas phase seems to equal the local oxygen potential in the oxide phase. The high local potential of sulfur along the crack or the pore results in the formation of sulfide. When the physical defects are large, relatively large areas of bare alloy are exposed directly to the bulk gas phase; so that degradation is similar to simple sulfidation attack and, in time, becomes severe.

Mari, et al.⁹ found that the sulfidation behavior of Fe-Cr-Al alloys after preoxidation to form Al_2O_3 was dependent on the potential of sulfidizing species in the sulfidation atmosphere. In pure sulfur, at lower pressure, a layered sulfide scale containing chromium and iron sulfides initially developed as a result of the diffusion of metal ions through the Al_2O_3 scale. On the other hand, sulfide nucleated and grew beneath the Al_2O_3 when the preoxidized alloy was exposed in $\text{H}_2/\text{H}_2\text{S}$ at atmospheric pressure.

Natesan¹ investigated the sulfidation/oxidation of preformed Cr_2O_3 scales on pure chromium. Specimens of pure chromium were preoxidized for 244 hours ($P_{\text{O}_2} = 9 \times 10^{-8}$ atm) and subsequently exposed for 120 hours to various oxygen-sulfur atmospheres ($P_{\text{O}_2} = 10^{-19}$, $P_{\text{S}_2} = 10^{-7}$ atm). Chromium sulfides were identified at the scale/gas interface by SEM without any evidence of sulfur transport into or through the oxide scale. It was concluded that the formation of the sulfide crystals on the external surface was largely controlled by chromium diffusion through the oxide scale. Detailed observations of the scale/alloy interface were not presented.

Perkins² and Huang, et al.¹⁰ reported that on Fe-Cr alloys, the outward transport of cations through the chromium oxide scale was dominant and led to the

formation of chromium sulfides on the surface of preoxidized specimens, even when the gas composition fell in the chromium oxide stable region of the Cr-S-O system.

Stott, et al.^{3,7} first reported the adverse effect of yttrium on the degradation of preformed oxide scales (Cr_2O_3 or Al_2O_3) in a sulfur-bearing environment for Fe-Cr-Al and Fe-Cr alloys with and without the addition of small amounts of yttrium exposed at 750°C in $\text{H}_2/\text{H}_2\text{O}/\text{H}_2\text{S}$ gas mixtures. Preoxidation to develop Al_2O_3 on Fe-Cr-Al and similar alloys containing yttrium gives a very significant improvement in corrosion resistance on subsequent exposure to equilibrated $\text{H}_2/\text{H}_2\text{O}/\text{H}_2\text{S}$ gases at 750°C . Breakdown of the preformed oxide scales on the Cr_2O_3 -forming alloys occurred at a much earlier stage than on the Al_2O_3 -forming alloys. It was also observed that some sulfide nodules developed relatively rapidly on the yttrium containing alloys. Sulfide nodules were usually formed over the area where second phase yttrium-rich precipitates (YFe_9) were located at or near the surface. It was concluded that the oxidation of the yttrium-rich phase results in an increase in localized Fe ion activity near the scale/gas interface. Also, oxidation of the yttrium-rich phase to Y_2O_3 is associated with a 9.1% increase in volume which could create further localized scale defects. The addition of reactive elements such as Y and Hf to the alloys improves the scale adherence and integrity during high temperature oxidation. However, their presence in the alloys may influence the degradation of the preformed oxide scale upon exposure to sulfur-bearing environments, but these effects are not well understood.

There are several questions regarding scale breakdown by sulfur that are not universally resolved. These include: i) whether the sulfur (and metallic) ions penetrate the scale by lattice diffusion, short-circuit diffusion, or transport

through physical defects; ii) whether sulfides nucleate at the scale/alloy interface or scale/gas interface; and iii) how sulfides grow. It is possible to form short-circuit diffusion paths for cations and/or anions or physical defects during the growth of oxide or in the period between preoxidation and subsequent exposure to sulfur-bearing gases. The resistance of preformed oxides to degradation in high PS_2 atmospheres may be expected to be intimately related to these defects.

EXPERIMENTAL

The alloys (Ni-30Cr, Fe-18Cr-6Al-1Hf, Fe-18Cr-6Al and Ni-20Si)* were prepared from 99.9% pure raw materials by arc melting in argon and drop casting in a chilled copper mold, 9.5 x 25.4 x 152.4 mm in size. The ingots were homogenized at 1100°C for 100 hours in an argon gas stream. Test specimens, approximately 12 x 9 x 2 mm in size, were ground on all surfaces through 600 grit on wet silicon carbide papers and ultrasonically cleaned in methanol.

Sulfidation/oxidation experiments were carried out at 950°C in $\text{H}_2/\text{H}_2\text{O}/\text{H}_2\text{S}$ gas mixtures with $\text{PS}_2=10^{-6.1}$ and $\text{PO}_2=10^{-14.7}, 10^{-17}, 10^{-18.7}$ atm. For reference, the positions of these gas compositions have been indicated on the thermodynamic stability diagrams for Al, Si, Cr, Fe, Ni and Hf in Figure 1.^{11,12} The $\text{H}_2/\text{H}_2\text{S}/\text{H}_2\text{O}$ gas mixtures were prepared by mixing 2.02% H_2S in H_2 , H_2 and Ar gases which were controlled by measuring each individual gas flow with precision flow meters. Water vapor was supplied to the gas mixture by bubbling argon gas through a water bath at constant temperature to produce a saturated gas of the desired water vapor content. Total gas flow was 200 cc/min. An electrical heating tape surrounded the tubing to the furnace to prevent condensation loss of water vapor. A platinum coated alumina honeycomb was placed in the reaction chamber to ensure

* Alloy compositions are given in weight percent.

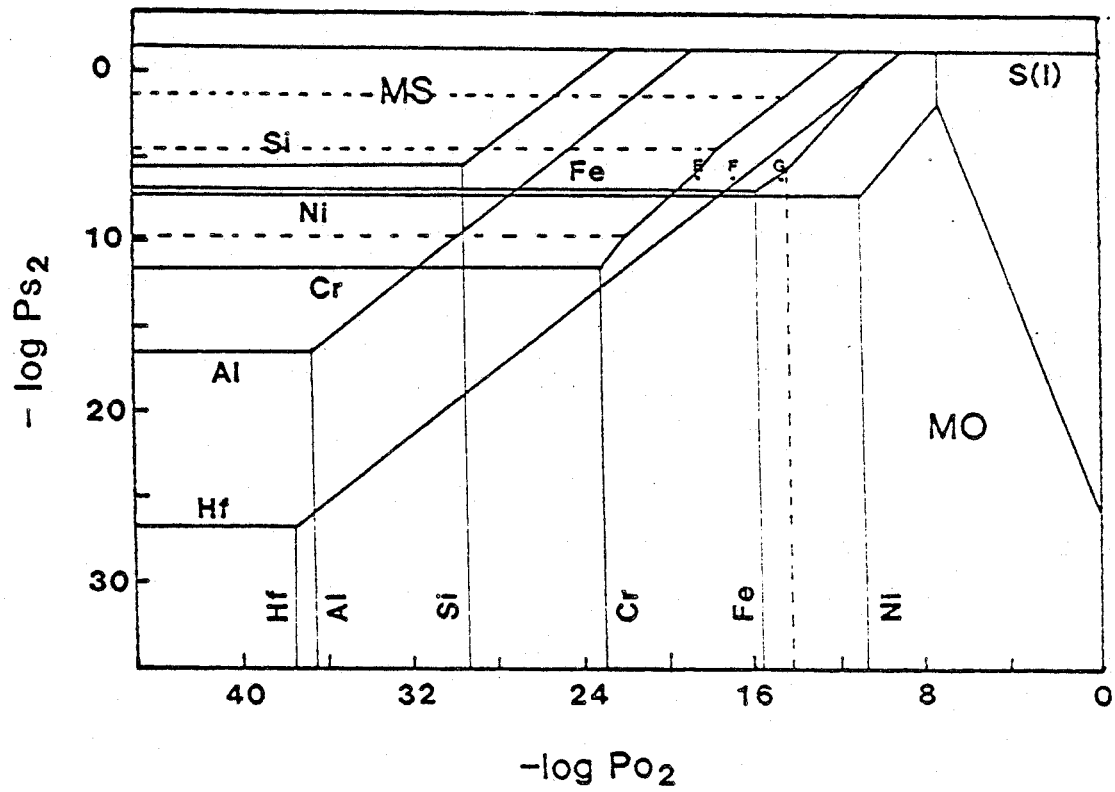


Figure 1: Stability Diagrams for the M (Al, Si, Cr, Fe, Ni and Hf)-S-O systems at 950°C. Gas compositions 'E, F and G' are illustrated.

equilibrium in the gas mixture. The gas compositions and the corresponding equilibrium partial pressures of oxygen and sulfur at 950°C are listed in Table I.

The experimental apparatus allowed specimens to be preoxidized in H₂/H₂O or air and subsequently exposed to equilibrated H₂/H₂S/H₂O gas mixtures at the reaction temperature without opening the reaction chamber. Specimens were held in the reaction chamber outside the furnace, while the system was flushed with nitrogen gas for 20 minutes following which the gas was switched to an equilibrated H₂/H₂S/H₂O or H₂/H₂O gas mixture. After equilibrium of the gas mixture was obtained, the specimen was moved to the hot zone by a magnet. At the end of an experiment, the specimen was pulled out to the cold zone. The temperature of the furnace was held constant within $\pm 2^\circ\text{C}$ during a run. After sulfidation/oxidation experiments and prior to preoxidation experiments in sulfur-free environments, the apparatus was baked out at higher temperature than the reaction temperature for more than 24 hours to ensure the reaction chamber was free of sulfur.

An acoustic emission test¹³ was used to detect in-situ physical damage such as scale cracking or separation from the substrate during preoxidation.

Most of the reaction products were identified by X-ray diffraction (XRD) techniques. The surface morphology and cross section of the scales were examined by scanning electron microscopy (SEM) with energy dispersive x-ray analysis (EDX) and wave length dispersive analysis (WDX). Observation of the underside of the scale and alloy substrate were carried out on scales spalled from the alloys during cooling or mechanically pulled from the alloy by a Sebastian adherence test machine. Prior to examination in the SEM, specimens were coated with palladium by evaporation to prevent charging effects and to increase contrast. Transmission electron microscopy (TEM) and Auger electron spectroscopy (AES) were used to characterize the fine structure of the corroded layer on Ni-20Si. TEM specimens

Table 1: Conditions employed to obtain equilibrium partial pressures of O_2 and S_2 at $950^\circ C$ and 1 atm total pressure.

	PH ₂	PH ₂ O	PH ₂ S	P _{Ar}	log P _{O2}	log P _{S2}
A	0.980		0.020			-6.10
B	0.684	0.015		0.301	-18.71	
C	0.419	0.064		0.517	-17.02	
D	0.194	0.411		0.395	-14.74	
E	0.672	0.015	0.012	0.301	-18.71	-6.10
F	0.412	0.064	0.007	0.517	-17.01	-6.10
G	0.190	0.412	0.003	0.395	-14.72	-6.10

were prepared by a back-thinning electropolishing technique which removes the alloy substrate and leaves a thin oxide layer. A 13% hydrochloric acid and 87% methanol solution was used at -50°C .

RESULTS

Microstructures of the Alloys

Figure 2 shows microstructures of three alloys (Ni-30Cr, Fe-18Cr-6Al-1Hf and Ni-20Si) which were homogenized at 1100°C for 100 hours. Ni-30Cr is an fcc single phase with chromium in solid solution. The grain size is 200-300 microns.

Fe-18Cr-6Al-1Hf is single phase ferrite with chromium and aluminum in solid solution with small amounts of Hf intermetallic compounds (HfFe_2). The distribution of these compounds is shown in the lower micrograph of (b). The alloy has elongated grains, which are characteristic of drop cast materials.

Ni-20Si consists of two constituents which are δ -phase (Ni_2Si) and a mixture of δ and Ni_3Si_2 phases, as identified by XRD. The smooth-appearing regions correspond to the δ -phase, while grainy regions correspond to $\delta + \text{Ni}_3\text{Si}_2$ presumably formed by eutectoid decomposition of the high temperature θ -phase. (Published phase diagrams for the Ni-Si systems are questionable in this concentration range.)

Sulfidation

Specimens of Ni-30Cr, Fe-18Cr-6Al-1Hf and Ni-20Si were exposed to a sulfidizing atmosphere (gas composition 'A') at 950°C . The weight changes for the three alloys after 4 hours of sulfidation correspond to:

$$\text{Ni-30Cr} \text{-----} \Delta m/A = 114.3 \text{ mg/cm}^2$$

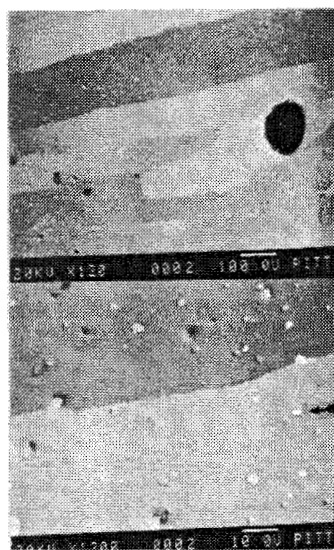
$$\text{Fe-18Cr-6Al-1Hf} \text{-----} \Delta m/A = >23.3 \text{ mg/cm}^2$$

$$\text{Ni-20Si} \text{-----} \Delta m/A = - 4.5 \text{ mg/cm}^2$$

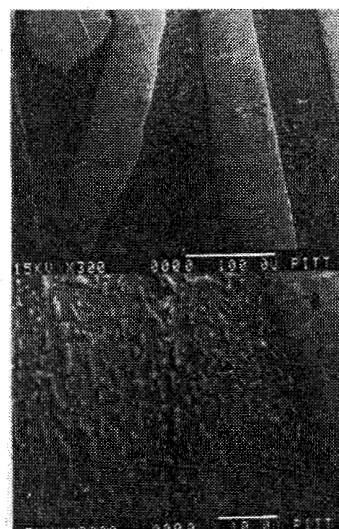
The corresponding sulfidation morphologies are presented in Figure 3. No attack



(a)



(b)



(c)

Figure 2: Microstructures of (a) Ni-30Cr, (b) Fe-18Cr-6Al-1Hf and (c) Ni-20Si after 100 hours of homogenization at 1100°C in Ar stream.

was apparent on Ni-20Si, as shown in (a) of Figure 3. However, the higher magnification micrographs of (a) and (b) of Figure 4 revealed significant amounts of porosity on the surface and deep penetration of these pores into the alloy, as shown in (c) and (d) of Figure 4. The formation of porosity and the penetration into the alloy appear to be related to the weight loss and suggest the evaporation of some components in the alloy because cracking or spalling was not observed.

Fe-18Cr-6Al-1Hf exhibited spalling of the external sulfide scales and severe degradation even in the alloy substrate, as shown in (b) of Figure 3. The scales formed on Fe-18Cr-6Al-1Hf were of a multilayer type consisting of an outer layer of isolated needles and blades and intermediate and inner layers of relatively compact and porous sulfides, respectively, as shown in Figure 5. The inner layer adjacent to the alloy surface showed scale separation in which small sulfide grains existed. Internal sulfides were also observed along the alloy grain boundaries. The outermost regions of the inner layer exhibited small pores arising from pores between the sulfide grains. The outer layer was comprised of iron sulfides and the inner and intermediate layers contained (Cr,Al) sulfides.

The sulfidized specimen of Ni-30Cr, which showed the worst sulfidation resistance among the three alloys, showed a voluminous sulfidation attack, (c) of Figure 3. The upper micrograph (c) shows the side of the specimen and the lower one the top of the same specimen. The sulfidized Ni-30Cr specimen exhibited an increase in volume approximately three times that of the original specimen. When the specimen was pulled from the hot zone of the furnace, the reaction products found on the surface were in a liquid state. Figure 6 shows the transverse section of the sulfidized Ni-30Cr specimen from (c) of Figure 3. The reaction products on Ni-30Cr were comprised of Cr sulfides (dark nodules), nickel sulfides (grey phases in the scale) and metallic nickel (brighter phases in the scale).

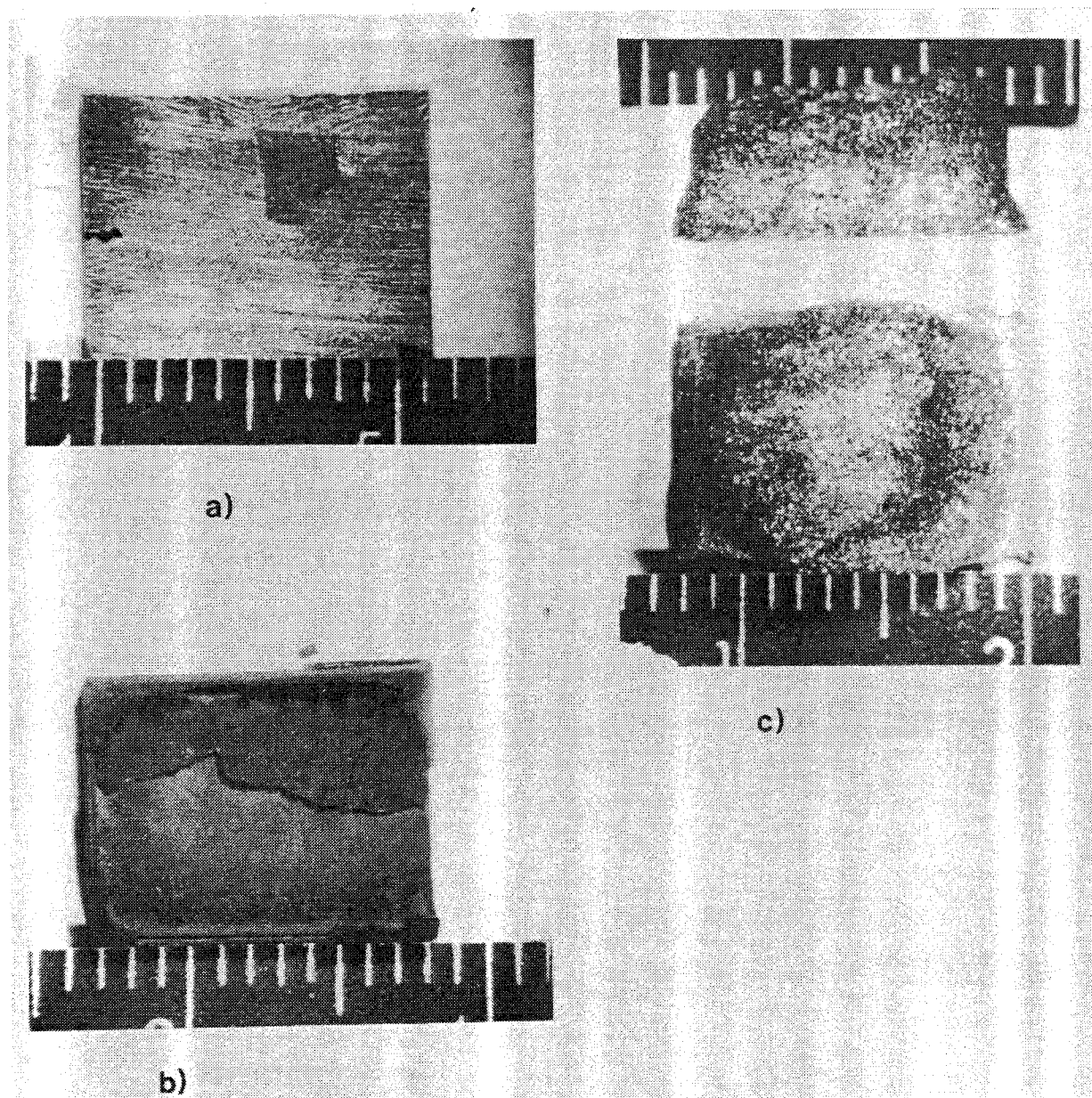


Figure 3: Sulfidized specimens in gas composition 'A' at 950°C for 4 hours. (a) Ni-20Si, (b) Fe-18Cr-6Al-1Hf and (c) Ni-30Cr.

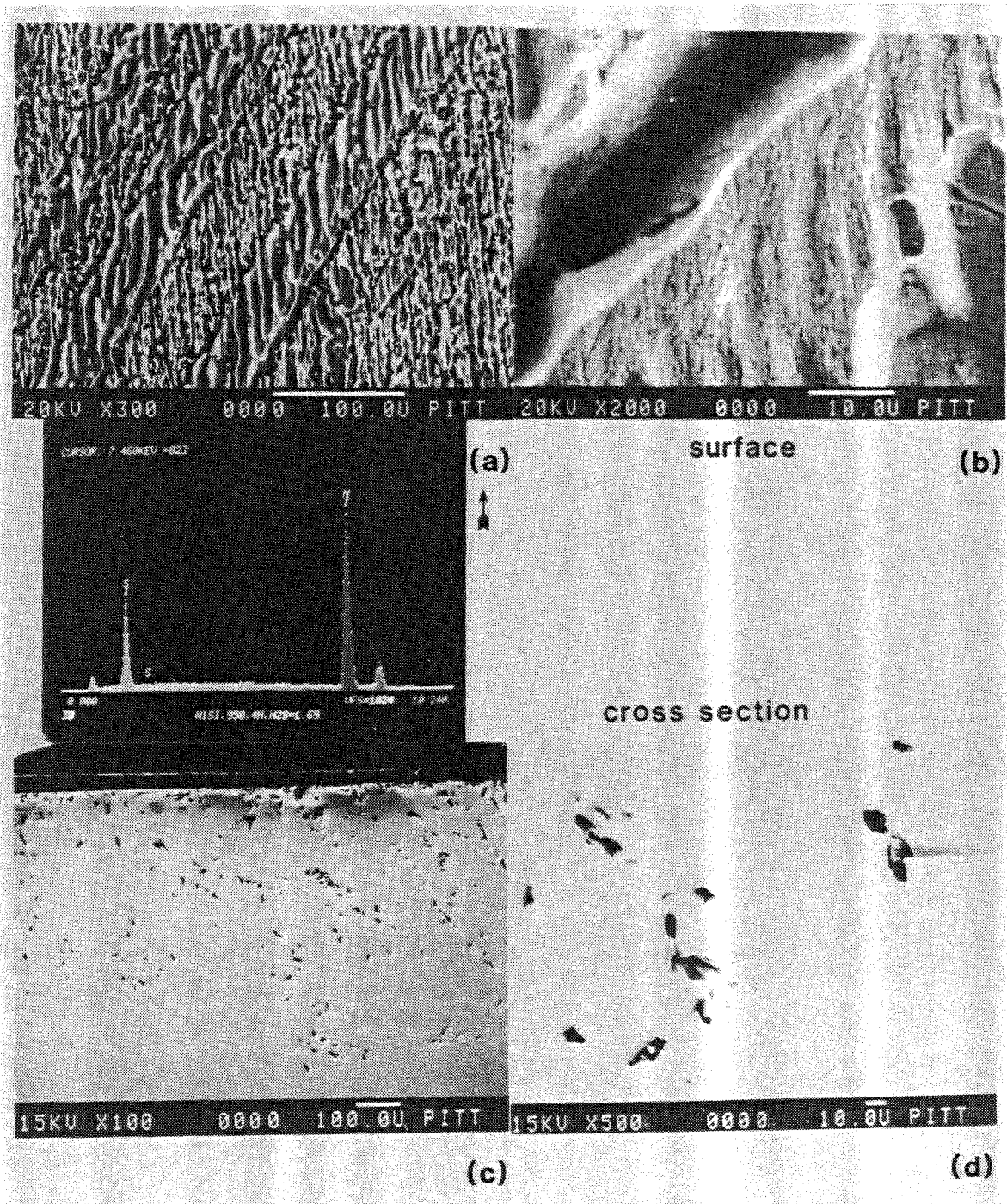


Figure 4: Higher magnification micrographs of (a) of Figure 3 and the transverse section of the specimen. (a)(b) alloy surface and (c)(d) the transverse section.

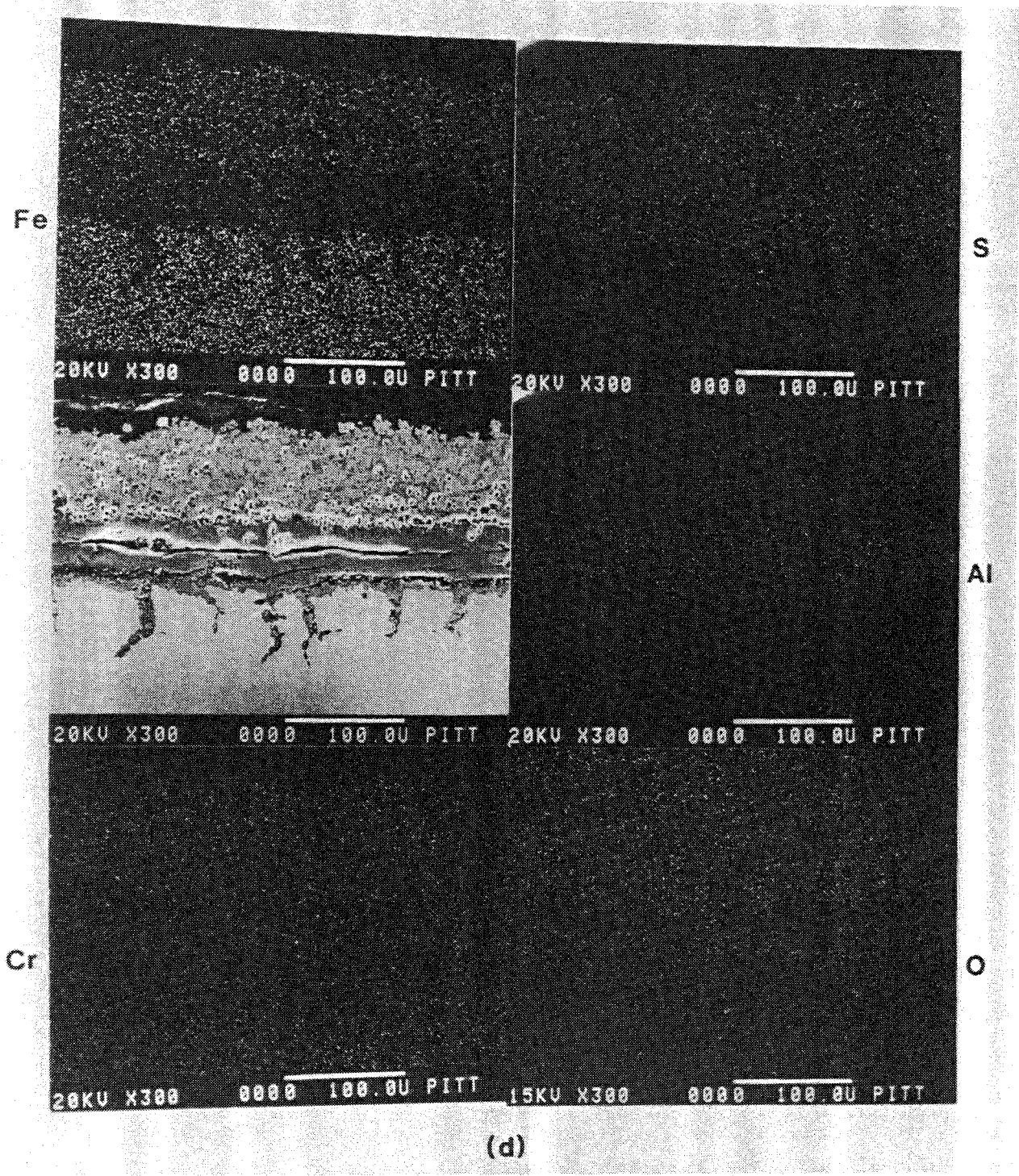


Figure 5: Transverse section of sulfidized Fe-18Cr-6Al-1Hf in gas composition 'A' at 950°C for 4 hours.

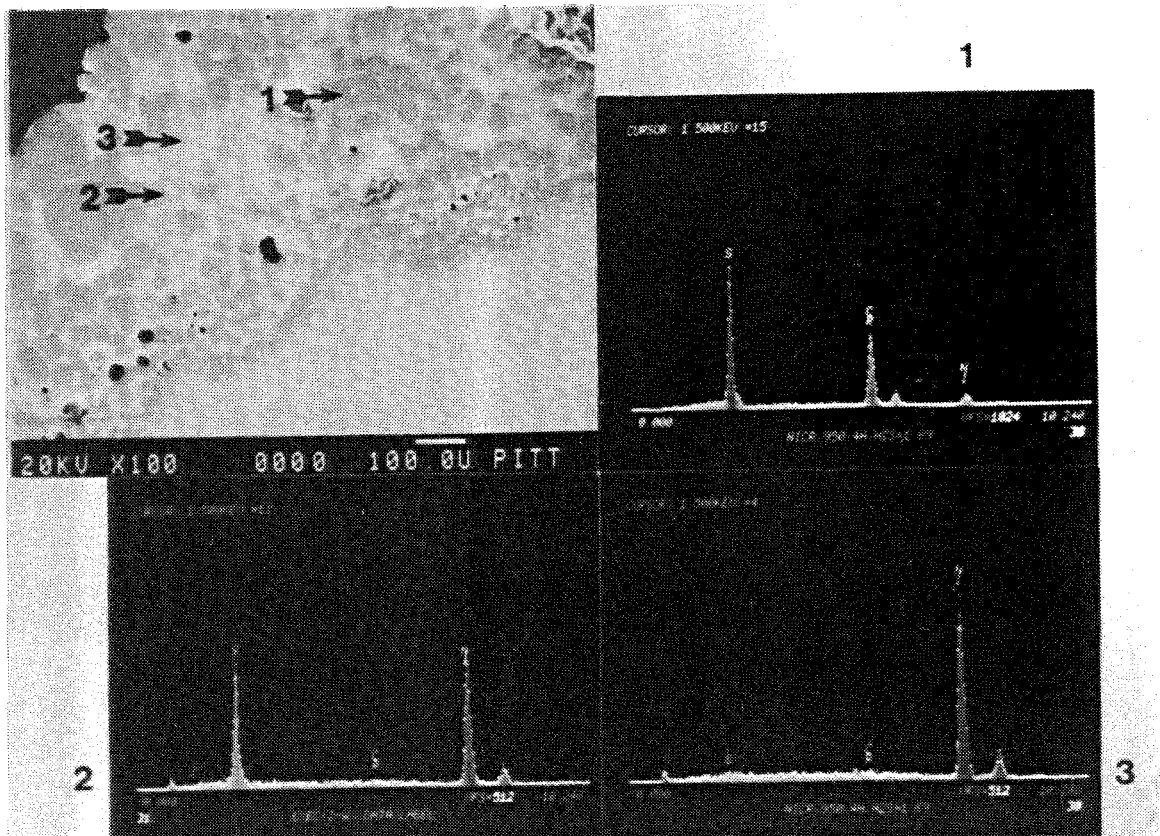


Figure 6: Transverse section of the sulfidized Ni-30Cr specimen in gas composition 'A' at 950°C for 4 hours.

Breakdown of Preformed Oxide Scales

The degradation resistance of high temperature alloys and coatings can be improved by the preformation of protective oxide scales, such as Cr_2O_3 , Al_2O_3 and SiO_2 . In these experiments, all specimens were preoxidized for 30 minutes at 950°C to provide preformed oxide scales on the alloy surface prior to exposure to sulfur-bearing gases unless otherwise specified. Table 2 shows how the preoxidation treatment can improve the degradation resistance to subsequent sulfidation/oxidation. The first column shows weight gains after sulfidation (gas composition "A") at 950°C for 4 hours. These have been discussed in the previous section. The next two columns indicate the weight changes after preoxidation treatments for 30 minutes at two different temperatures, 950 and 1150°C (gas composition "B"). The last three columns are the weight changes of the specimens which were exposed to gas composition "E" for 4 hours at 950°C , one without preoxidation and two with different preoxidation treatments at 950 and 1150°C for 30 minutes. Preoxidation was observed to reduce the sulfidation attack of all three alloys. For Ni-30Cr, with the higher temperature preoxidation, less weight gain was obtained but for Fe-18Cr-6Al-1Hf, more weight gain resulted. This means that the Cr_2O_3 scale formed on Ni-30Cr becomes more protective to sulfidation/oxidation with higher temperature preoxidation apparently because a thicker scale is produced as the preoxidation temperature increases. On the other hand, the Al_2O_3 scale formed on Fe-18Cr-6Al-1Hf becomes less protective to sulfidation/oxidation with high temperature preoxidation. This implies that the degradation of the Al_2O_3 could occur by mechanical damage rather than diffusive processes. The sulfidation resistance of Ni-20Si was excellent regardless of the preoxidation temperature. Small pores were observed on the alloy surface even after preoxidation. This will be discussed in a later section.

Table 2: Weight changes after 4 hours of sulfidation-oxidation at 950°C.

	log PS2= -6.10	log PO2= -18.71 950 C 30 min	log PO2= -15.30 1150 C 30 min	log PO2= -18.71	log PS2= -6.10	
					preox 950 C,30 min	preox 1150 C,30 min
Ni-Cr	114.30	0.10	0.64	55.74	20.20	1.09
Fe-Cr-Al-Hf	23.25	negligible	0.11	5.90	0.35	0.48
Ni-Si	-4.53	-0.04	0.03	0.10	0.04	0.04

In general, the protectiveness of alloys was significantly improved by the preformation of the oxide scale, but eventually the scales broke down. The mechanisms of scale breakdown in high P_{S_2} atmospheres will now be discussed for the three oxides (Cr_2O_3 , Al_2O_3 and SiO_2).

Preformed Cr_2O_3 Scale

The Cr_2O_3 scale formed on Ni-30Cr had good adherence and integrity after 30 minutes of oxidation at $950^\circ C$ in gas composition 'B'. This alloy did not show any spalling of the scale on cooling from the reaction temperature. In order to examine the scale/alloy interface, oxide scales were separated from the alloy substrate by breaking the oxide layer. The morphologies of the external scale and the alloy substrate are shown in Figure 7. A considerable number of voids was observed on the alloy substrate. Also, the same distribution of dimples was observed on the surface of the oxide scale as on the alloy substrate. It is apparent that these dimples are on the top of voids in the alloy substrate. This suggests that the thickness of the oxide scale formed over the voids is thinner than that away from the voids.

Breakdown of Preformed Cr_2O_3 Scales

Specimens of Ni-30Cr which were oxidized in gas composition "B" at $950^\circ C$ for 30 minutes and subsequently exposed to sulfur-bearing gases (gas composition "E") at $950^\circ C$ for 5, 10 and 20 minutes without intermediate cooling to room temperature are shown in Figures 8, 9 and 10, respectively. The scale/alloy interfaces were examined by pulling the oxide scale from the alloy substrate using a Sebastian adherence test machine. No evidence of external sulfide formation on the oxide scale was observed after 5 minutes of sulfidation/oxidation, Figure 8. External sulfides at the scale/gas interface and internal sulfides at the scale/alloy interface were observed after 10 minutes of sulfidation/oxidation, Figure 9. In the



Figure 7: Morphologies of the external scale surface and the alloy substrate of Ni-30Cr after 30 minutes of oxidation in gas composition 'B' at 950°C.

early stages of sulfidation/oxidation, both external and internal sulfides were mainly chromium sulfides, however the external sulfides were alloyed with a small amount of Ni. External chromium sulfides were covered by a thin layer of chromium oxide and internal chromium sulfides were stuck to the underside of the oxide scale. The distribution of internal sulfides was similar to that of the voids, which had formed in the alloy substrate during preoxidation. In addition to small particles of internal sulfides on the underside of the scale, numbers of rims, also identified as chromium sulfides, were observed. The rims on the underside of the oxide scale appeared to grow to form internal sulfide particles, whose sizes were similar to those of the voids in the alloy substrate. This suggests that sulfur penetrates the Cr_2O_3 scale over the voids and nucleates internal sulfides preferentially at the the rims of voids where the activity of chromium is highest if chromium evaporation in the voids is negligible. The newly formed internal sulfides rims appeared to grow and eventually fill the voids. In order to check the relationship between the external sulfides and internal sulfides, the specimen, shown in Figure 9, was taper-polished, resulting in the removal of the external sulfides, shown in (a) of Figure 11. An arrow in this micrograph indicates a site where an external sulfide was located. The site is concave and contains sulfur as shown by EDX. These concave dimples have been observed after the preoxidation of Ni-30Cr. Therefore, the penetration of sulfur appears to occur preferentially through the oxide scale over the voids and eventually forms sulfide-rich channels through the preformed oxide scale. As the reaction progressed, the external sulfides became enriched in nickel and formed nickel sulfides on top of the initially formed chromium sulfides, as shown in Figure 10. These nickel sulfides are thermodynamically stable at the scale/gas interface. Figures 10 (b) and (c) are,

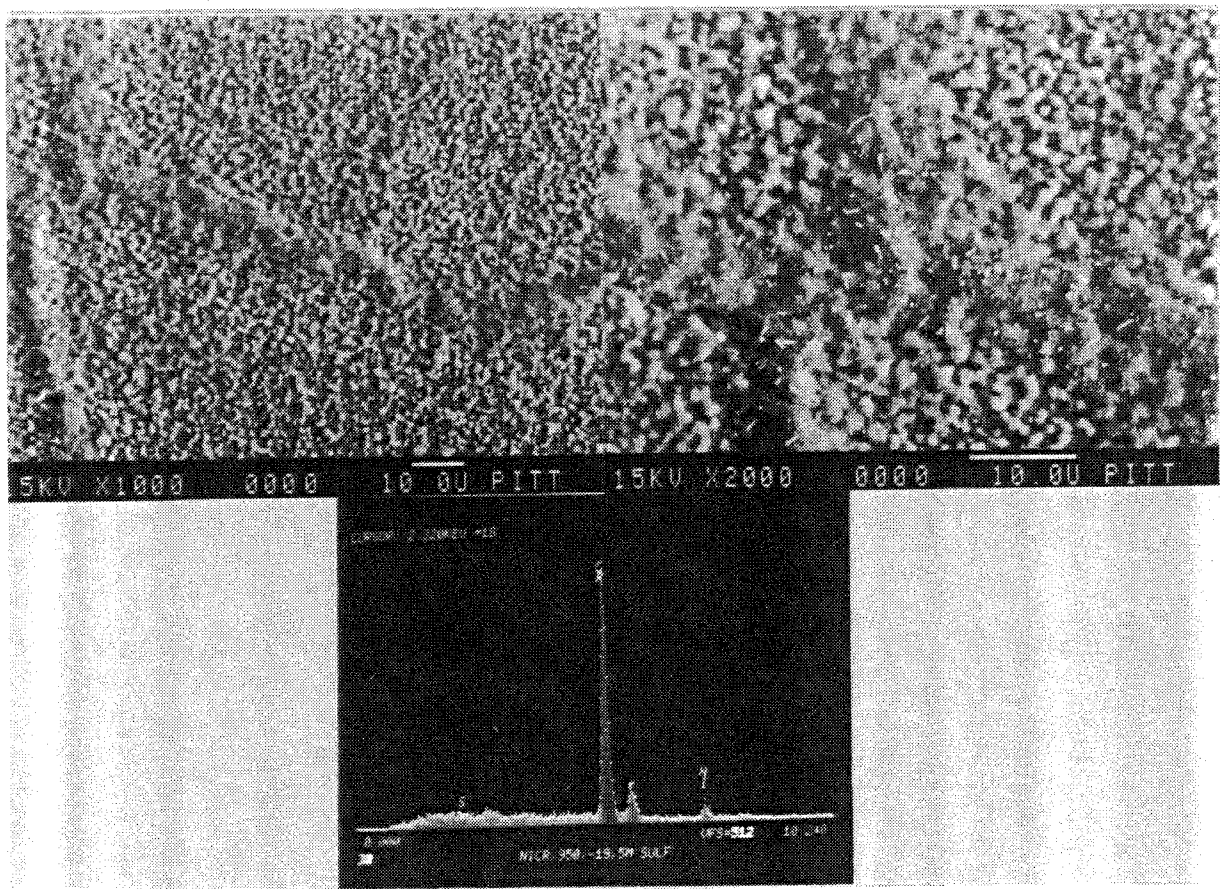


Figure 8: Ni-30Cr exposed to gas composition 'B' for 30 minutes and subsequently exposed to gas composition 'E' for 5 minutes at 950°C.

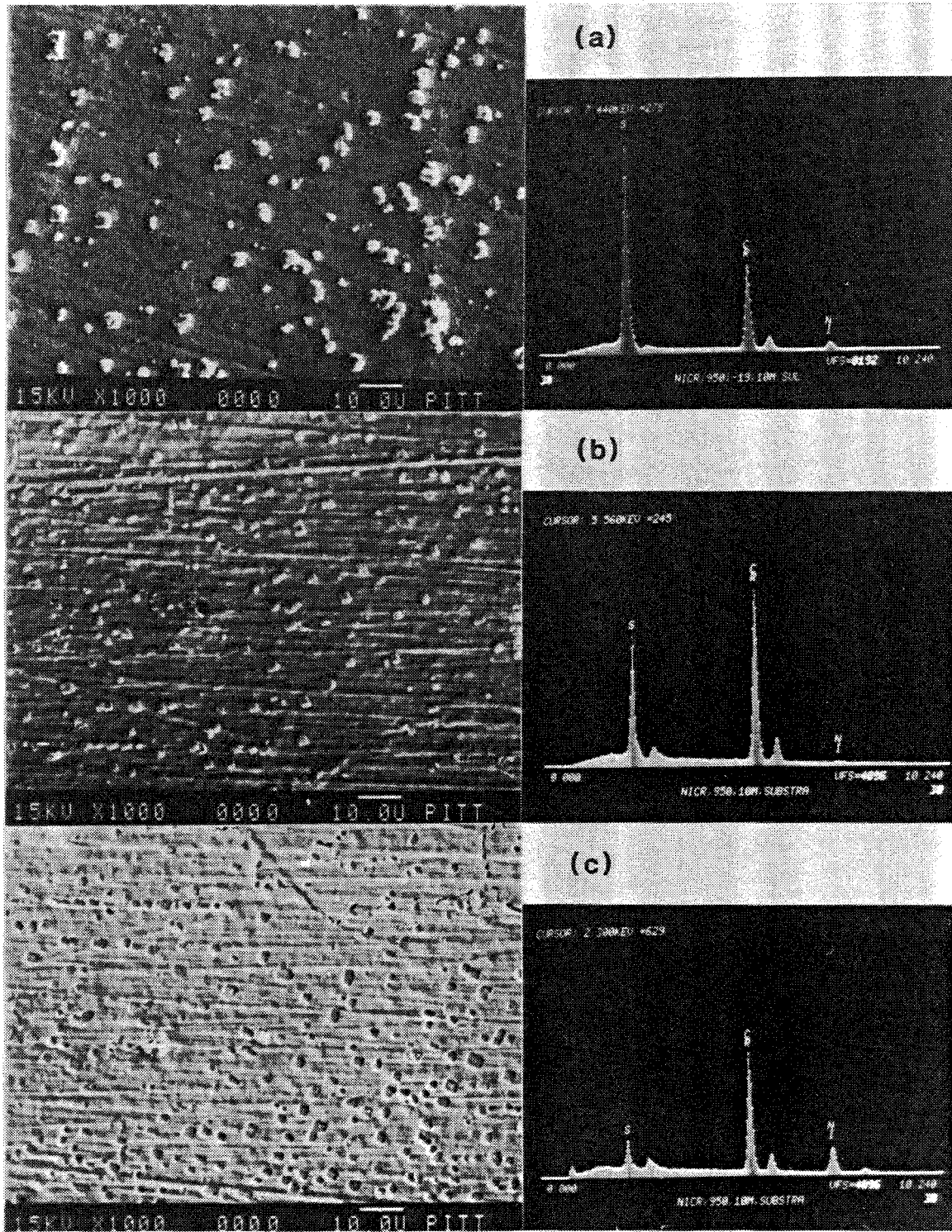


Figure 9: Ni-30Cr exposed to gas composition 'B' for 30 minutes and subsequently exposed to gas composition 'E' for 10 minutes at 950°C. (a) external oxide scale (b) underside of the oxide scale and (c) alloy substrate.

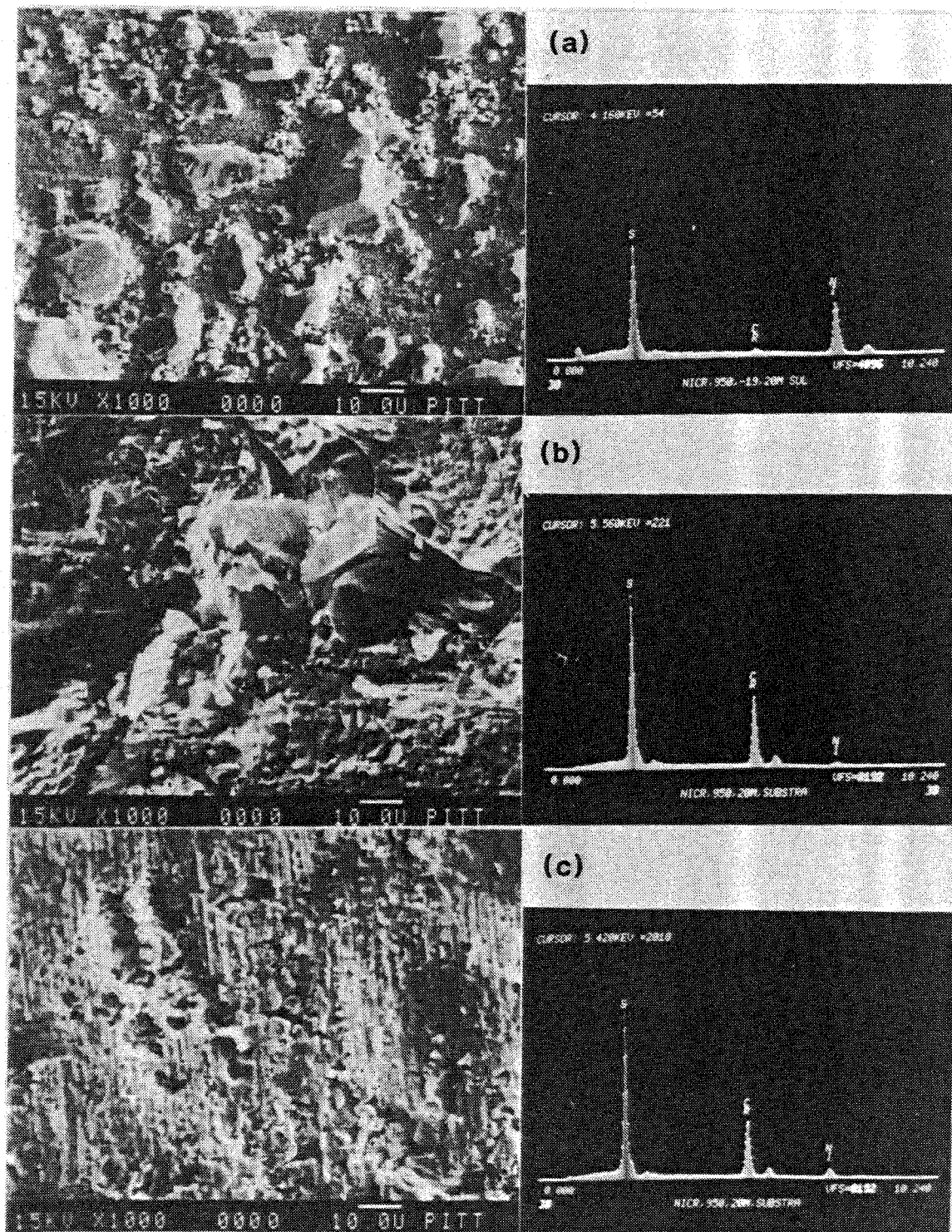


Figure 10: Ni-30Cr exposed to gas composition 'B' for 30 minutes and subsequently exposed to gas composition 'E' for 20 minutes at 950°C. (a) external oxide scale (b) underside of the oxide scale and (c) alloy substrate.

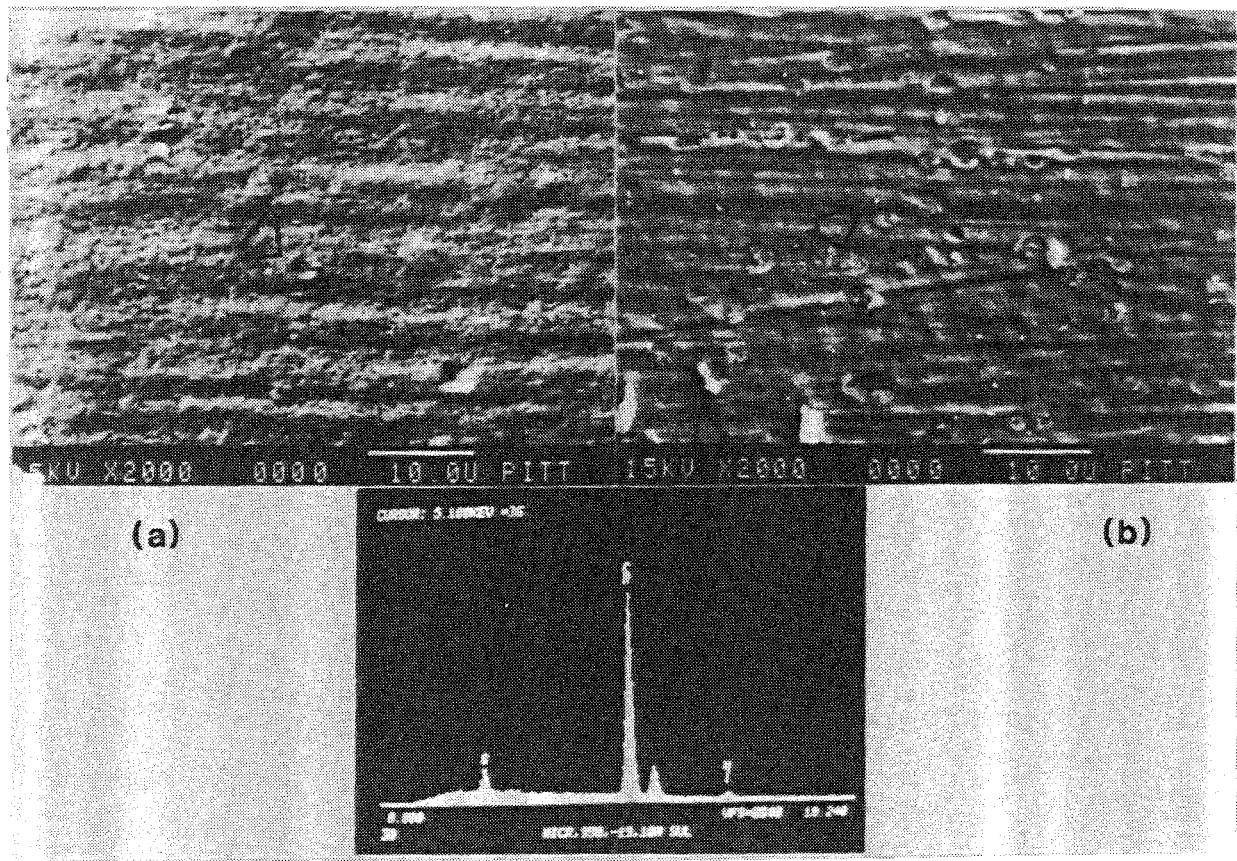


Figure 11: Taper polished Ni-30Cr which was exposed to gas composition 'B' for 30 minutes and subsequently exposed to gas composition 'E' for 10 minutes for 4 hours.
(a) taper polished external scale and
(b) underside of the oxide scale.

respectively, micrographs of the underside of the oxide scale and the alloy substrate which was severely degraded at this stage.

Preformed Al_2O_3 Scale

The Al_2O_3 scale layer formed on Fe-18Cr-6Al tended to spall after 30 minutes of oxidation in gas composition 'B' at 950°C . The scale formed was light green, which is the typical color of $\gamma\text{-Al}_2\text{O}_3$. This was confirmed by XRD and selected area electron diffraction patterns (SAD). The substrate exhibited numerous voids in the spalled areas, shown in Figure 12. These voids may cause the poor adherence of the oxide scale.

The Al_2O_3 scale formed on Fe-18Cr-6Al-1Hf was adherent after 30 minutes of oxidation at 950°C in gas composition 'B', as shown in (a) of Figure 13. XRD and EDX analysis on the surface of the scale revealed some hafnium oxides and metallic Fe as well as Al_2O_3 . Some hafnium oxide pegs were also observed on the underside of the Al_2O_3 layer, whose surface was relatively smooth. Some concave craters were observed in the substrate with Hf-rich oxide embedded in their center. Except for these craters, no distinct voids were observed, and the alloy substrate was fairly smooth.

Breakdown of Preformed Al_2O_3 Scales

Fe-18Cr-6Al-1Hf was preoxidized in gas composition "B" at 950°C for 30 minutes and subsequently exposed to gas composition "E" for 4 hours at the same temperature, Figure 14. Small white particles, identified as iron sulfides, were observed around HfO_2 in the Al_2O_3 scale. Comparatively large particles, identified as chromium sulfides and showing some oxygen in WDX analysis, were located beside the small sulfide particles. It is believed that sulfides form initially by sulfidation of metallic Fe around HfO_2 and that as the sulfidation/oxidation continues, the small iron sulfides are outgrown by chromium sulfides, covered by a

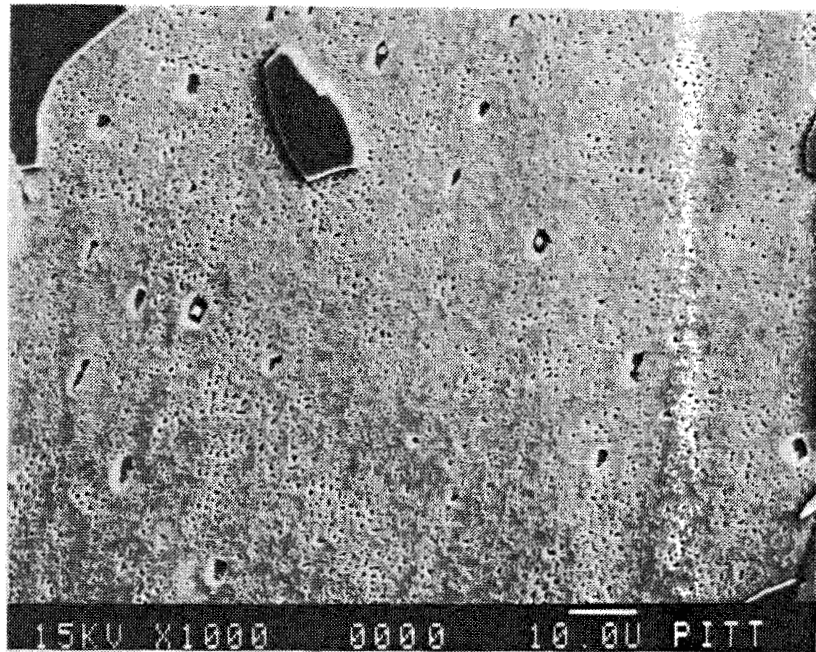


Figure 12: Morphologies of Fe-18Cr-6Al after 30 minutes of oxidation at 950°C in gas composition 'B'.

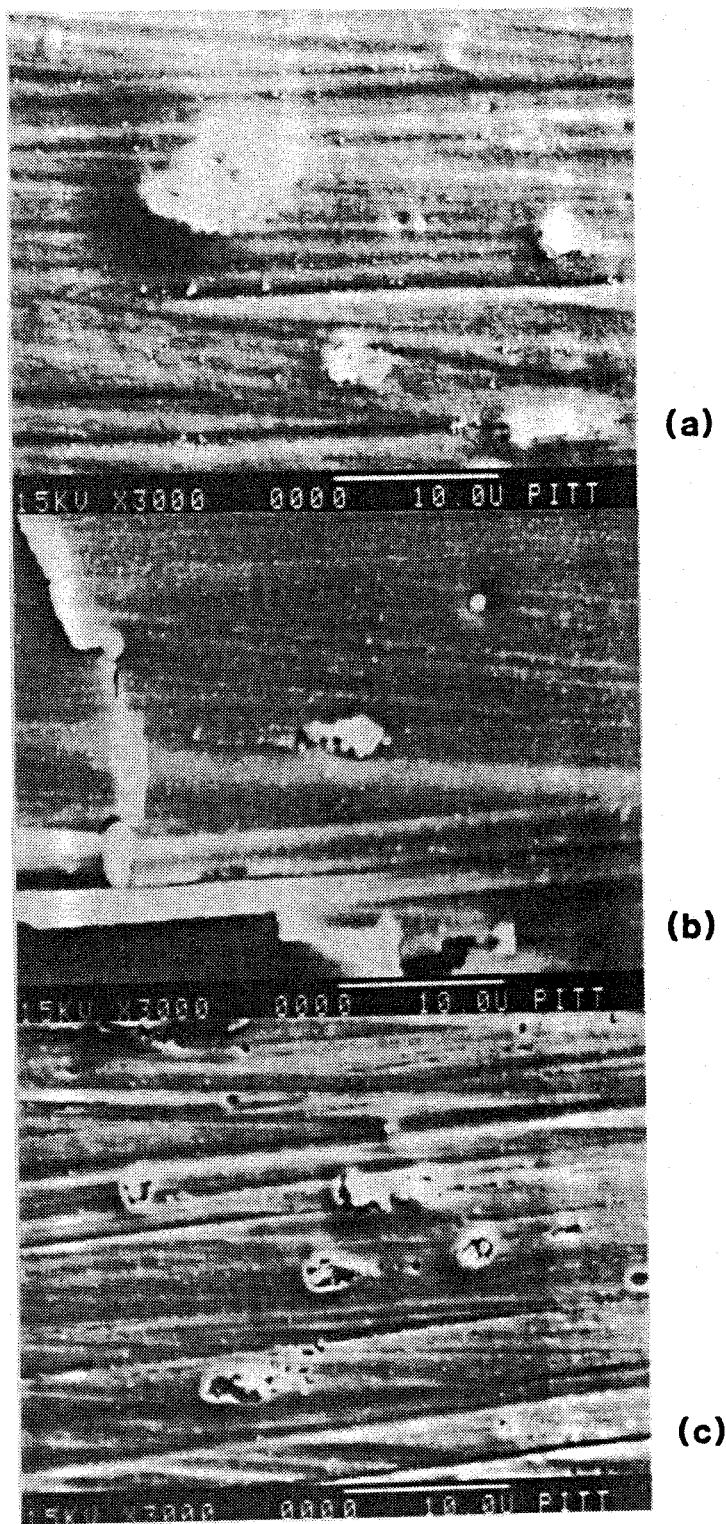


Figure 13: Morphologies of (a) the external scale surface, (b) the underside of scale and (c) the alloy substrate of Fe-18Cr-6Al-1Hf after 30 minutes of oxidation at 950°C in gas composition 'B'.

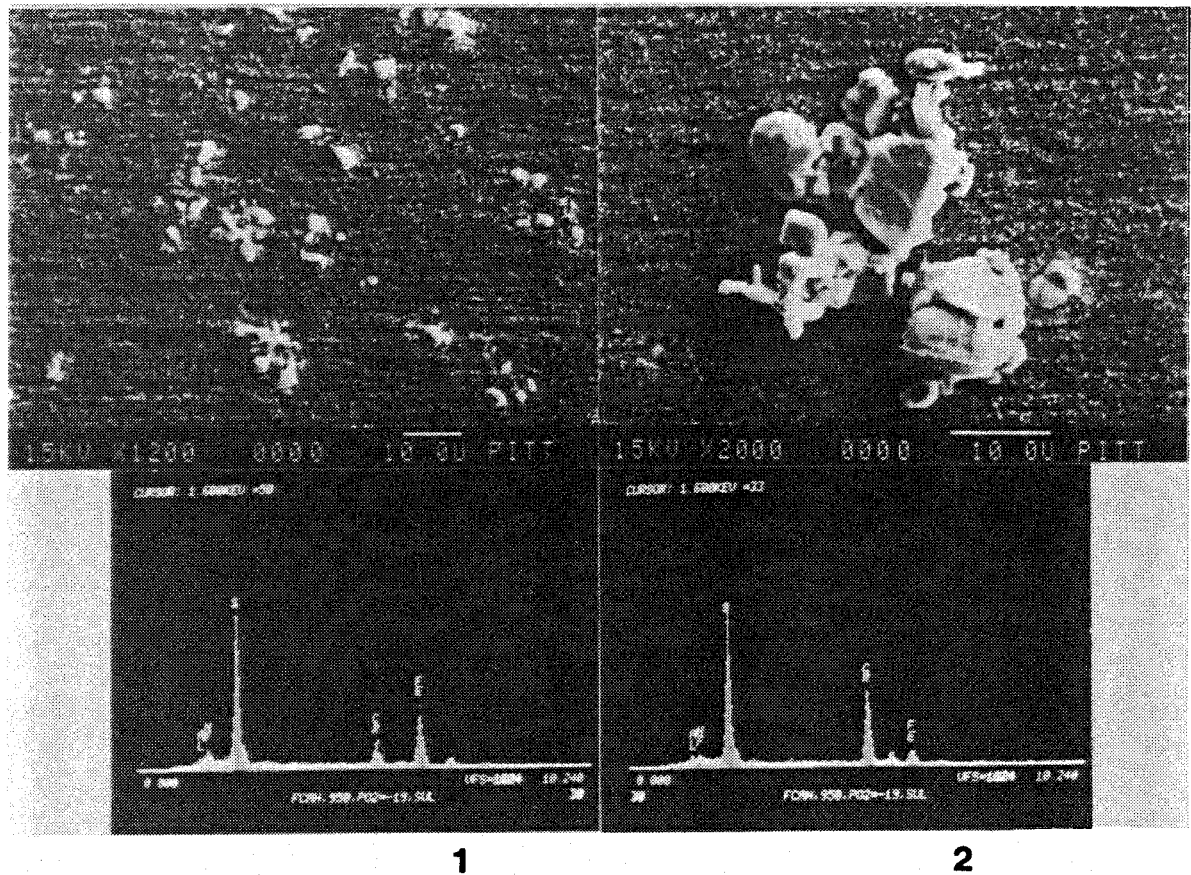


Figure 14: Surface morphologies of Fe-18Cr-6Al-1Hf exposed to gas composition 'B' for 30 minutes and subsequently exposed to gas composition 'E' for 4 hours.

thin layer of chromium oxide. Figure 15 shows an Al_2O_3 scale pulled off to examine the scale/alloy interface. The external oxide layer appeared to be protective except for the formation of iron sulfides around hafnium-rich regions. The underside of the Al_2O_3 scale, shown in (b) of Figure 15, revealed both sulfides and oxides. The oxide particles are mainly Al_2O_3 and hafnium oxides which have not been transformed to sulfides, and the sulfide particles are hafnium-rich sulfides, as shown in (b) of Figure 15. The preformation of the Al_2O_3 scale on Fe-18Cr-6Al-1Hf produced craters around hafnium oxide pegs, shown in (b) of Figure 13. Upon sulfidation-oxidation, the hafnium oxide pegs were reacted to hafnium-rich sulfides and the craters formed during the preoxidation were filled by these sulfides. Except for these sulfides, the oxide scale/alloy interface is relatively smooth and appears to be intact.

Figure 16 shows a further developed stage of the sulfidation-oxidation in the same gas composition 'E' at 950°C . The outermost sulfide layer was iron sulfide and beneath this layer a chromium sulfide layer was observed. Figure 17 shows the spalling of the oxide scale around a Hf-rich phase in the alloy substrate. From the results of the sulfide formation and the oxide scale failure around HfO_2 , it can be concluded that the sulfidation of Fe-18Cr-6Al-1Hf is closely related to the existence of Hf in the alloy.

For comparison, Fe-18Cr-6Al, exposed to the same experimental conditions as Fe-18Cr-6Al-1Hf, is shown in Figure 18. The numbers of external sulfide nodules were fewer but the sizes were significantly bigger compared to those on Fe-18Cr-6Al-1Hf. Except for the big sulfide nodules, the Al_2O_3 scale appeared to be smooth and protective.

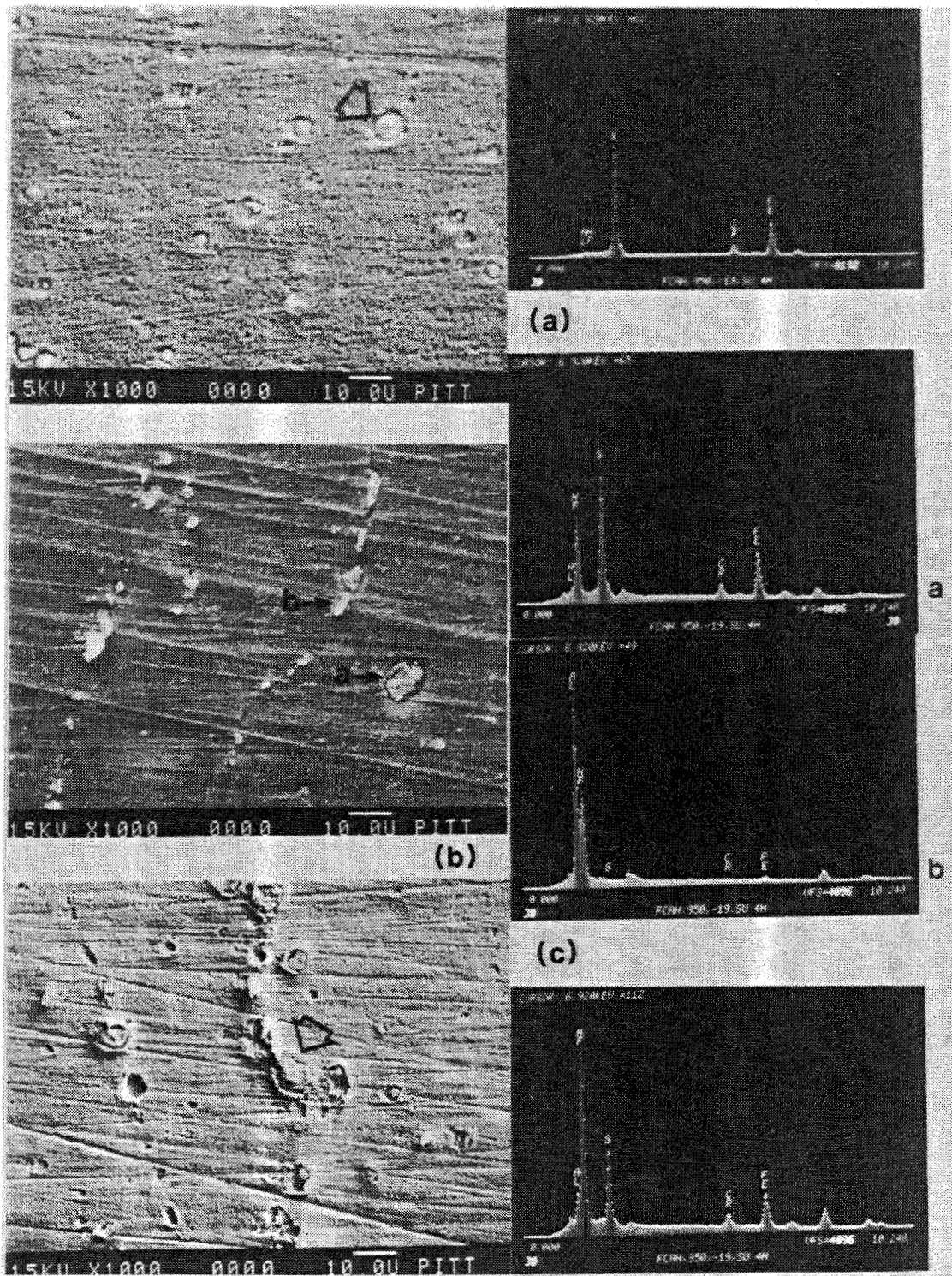


Figure 15: Fe-18Cr-6Al-1Hf exposed to gas composition 'B' for 30 minutes and subsequently exposed to gas composition 'E' for 4 hours at 950°C. (a) external oxide scale (b) underside of the scale and (c) alloy substrate.

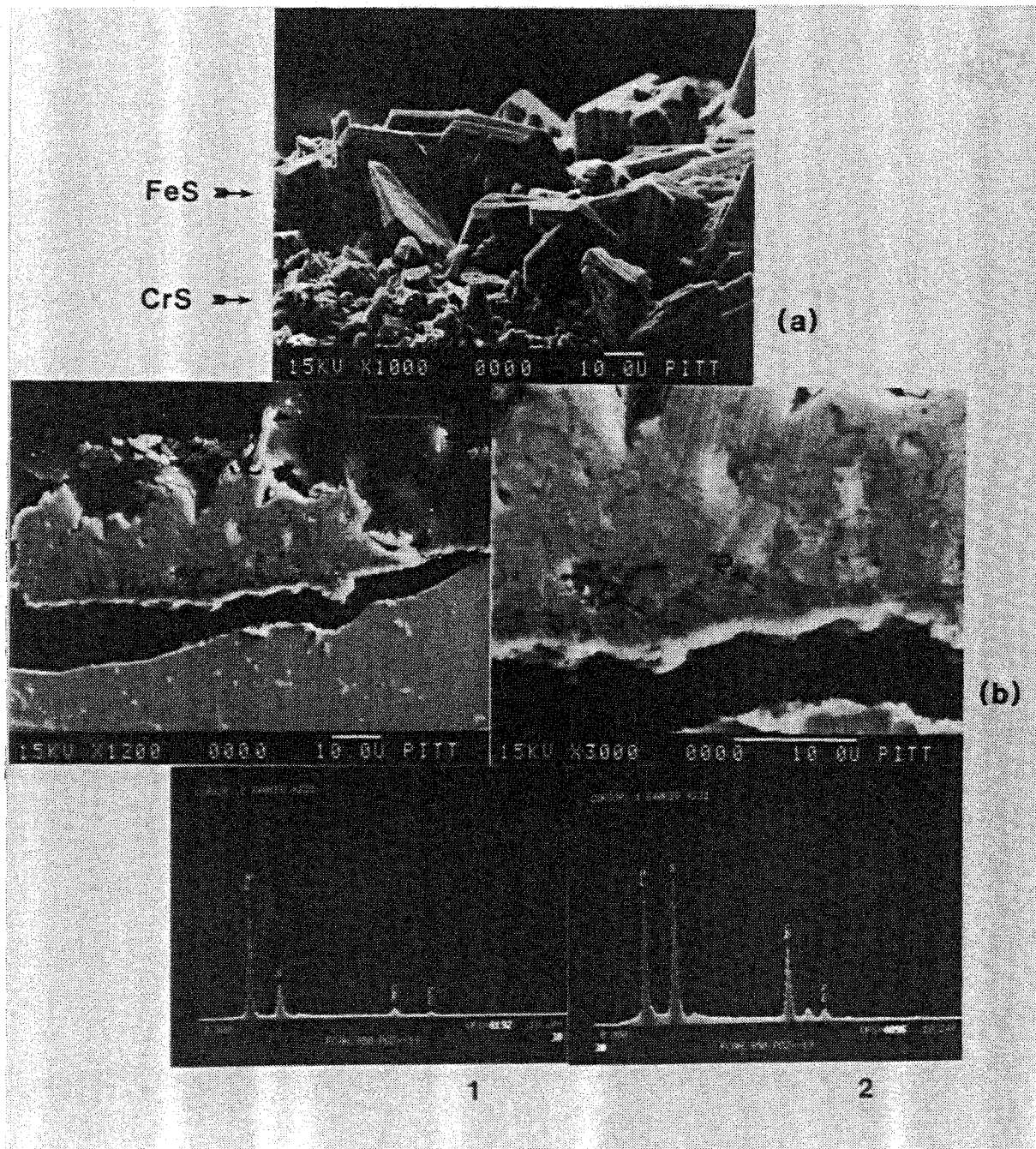


Figure 16: Fe-18Cr-6Al-1Hf exposed to gas composition 'B' for 30 minutes and subsequently exposed to gas composition 'E' for 4 hours at 950°C. (a) external sulfide morphology and (b) transverse section.

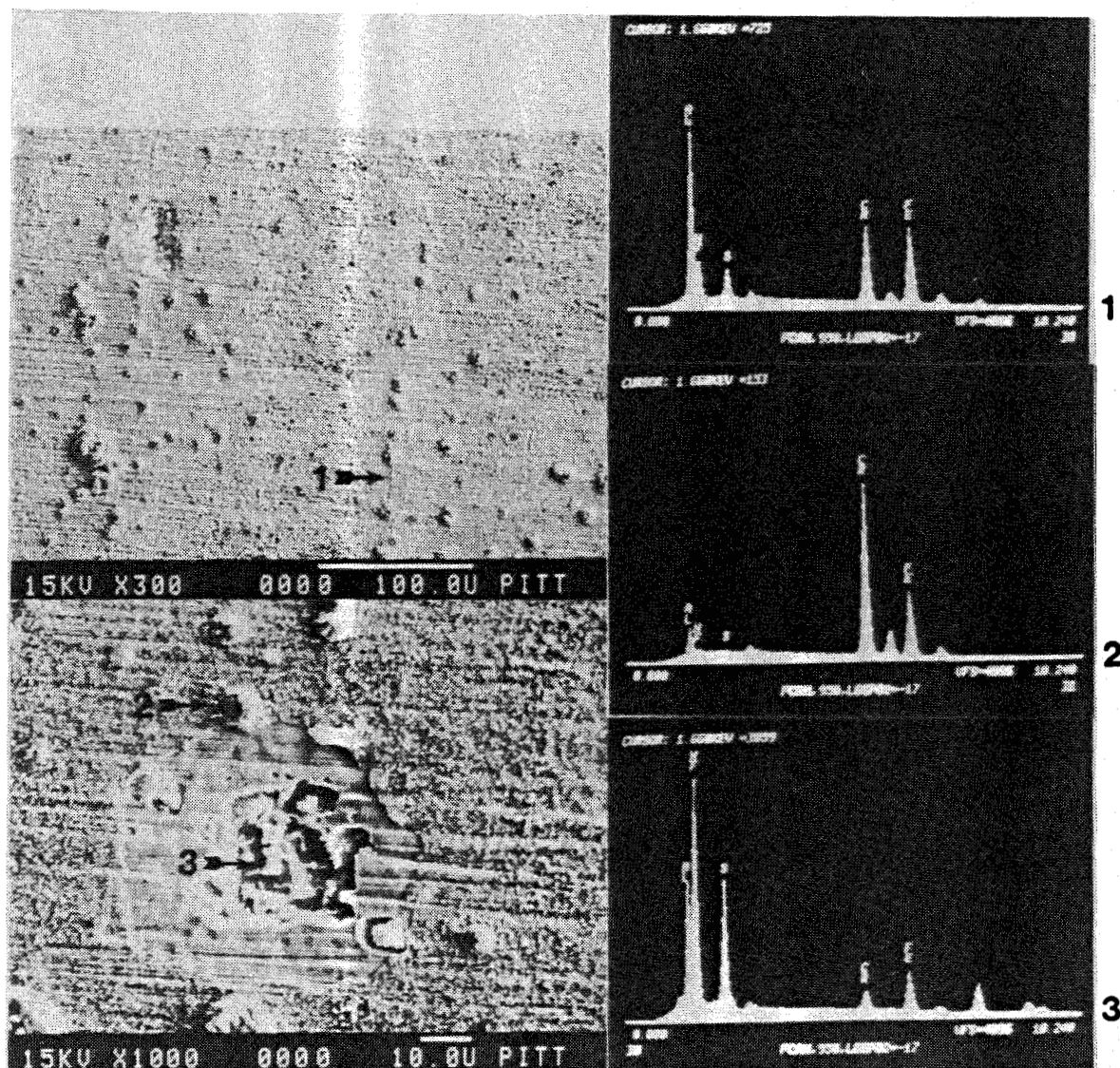


Figure 17: Fe-18Cr-6Al-1Hf exposed to gas composition 'B' for 30 minutes and subsequently exposed to gas composition 'F' for 4 hours at 950°C.

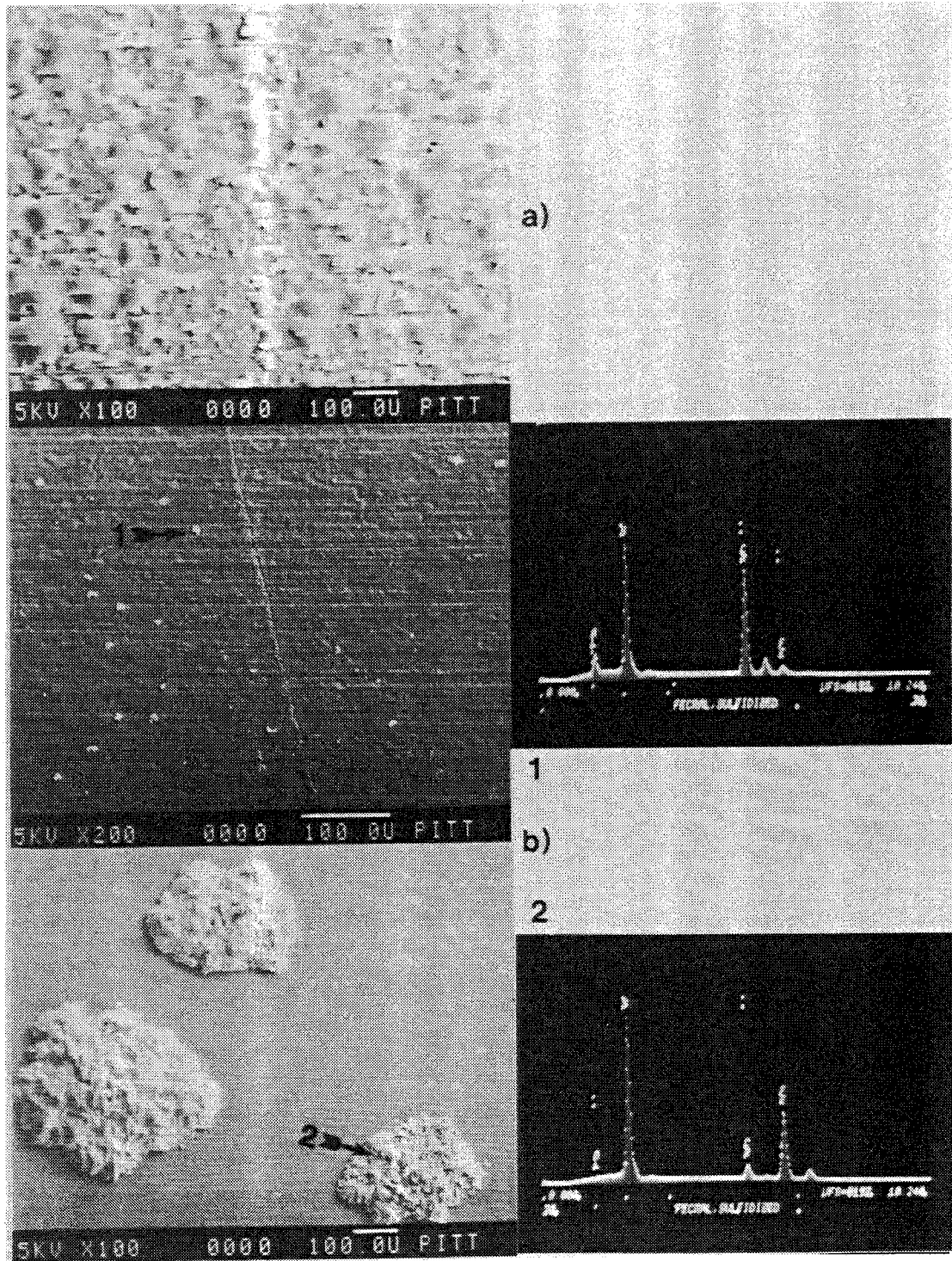


Figure 18: Fe-18Cr-6Al exposed to gas composition 'B' for 30 minutes and subsequently exposed to gas composition 'E' for 4 hours at 950°C. (a) after preoxidation and (b) after sulfidation-oxidation.

Preformed SiO₂ Scale

A thin layer of vitreous silica formed on Ni-20Si after oxidation at 950°C. Figure 19 is a transmission electron micrograph of the SiO₂ layer formed over the single phase δ and two-phase $\delta + \text{Ni}_3\text{Si}_2$ regions with the corresponding SAD patterns. The oxide layer is comprised of a clear vitreous silica layer along with transient oxide islands (Ni_2SiO_4), identified by SAD. It is apparent that a vitreous silica layer formed over the $\delta + \text{Ni}_3\text{Si}_2$ phases and more transient oxides formed over the δ -phases of the alloy (lower silicon content). To examine the scale/alloy interface, an oxide layer was mechanically stripped using the Sebastian adherence tester. Small pores were observed at the scale/gas interface, but generally the surface was featureless and smooth. Also, the scale/alloy interface was smooth with no indication of void formation. These results are shown in Figure 20.

Breakdown of Preformed SiO₂ Scales

Ni-20Si was preoxidized in gas composition "B" at 950°C for 30 minutes and subsequently exposed to gas composition "E" for 4 hours at the same temperature, Figure 21. No apparent sulfidation attack was observed and the appearance of the scale was quite similar to that on the preoxidized specimen. The wrinkles, shown in (a), were formed during SEM examination due to the bombardment of electrons on the very thin oxide scale deforming the scale. Apparently, the plasticity of the SiO₂ layer is substantial at high temperatures. This behavior has been also observed during thermal cycling at 950°C. No voids were observed at the scale/alloy interface and no degradation was observed at the scale/gas and scale/alloy interfaces unless cracks existed. Then nickel sulfide nodules, shown in Figure 22, were found at the scale/gas interface. The number of nodules was limited and nodules were always found along cracks, which existed in the alloy before exposure to the sulfur bearing gases. Porosity was observed in the external

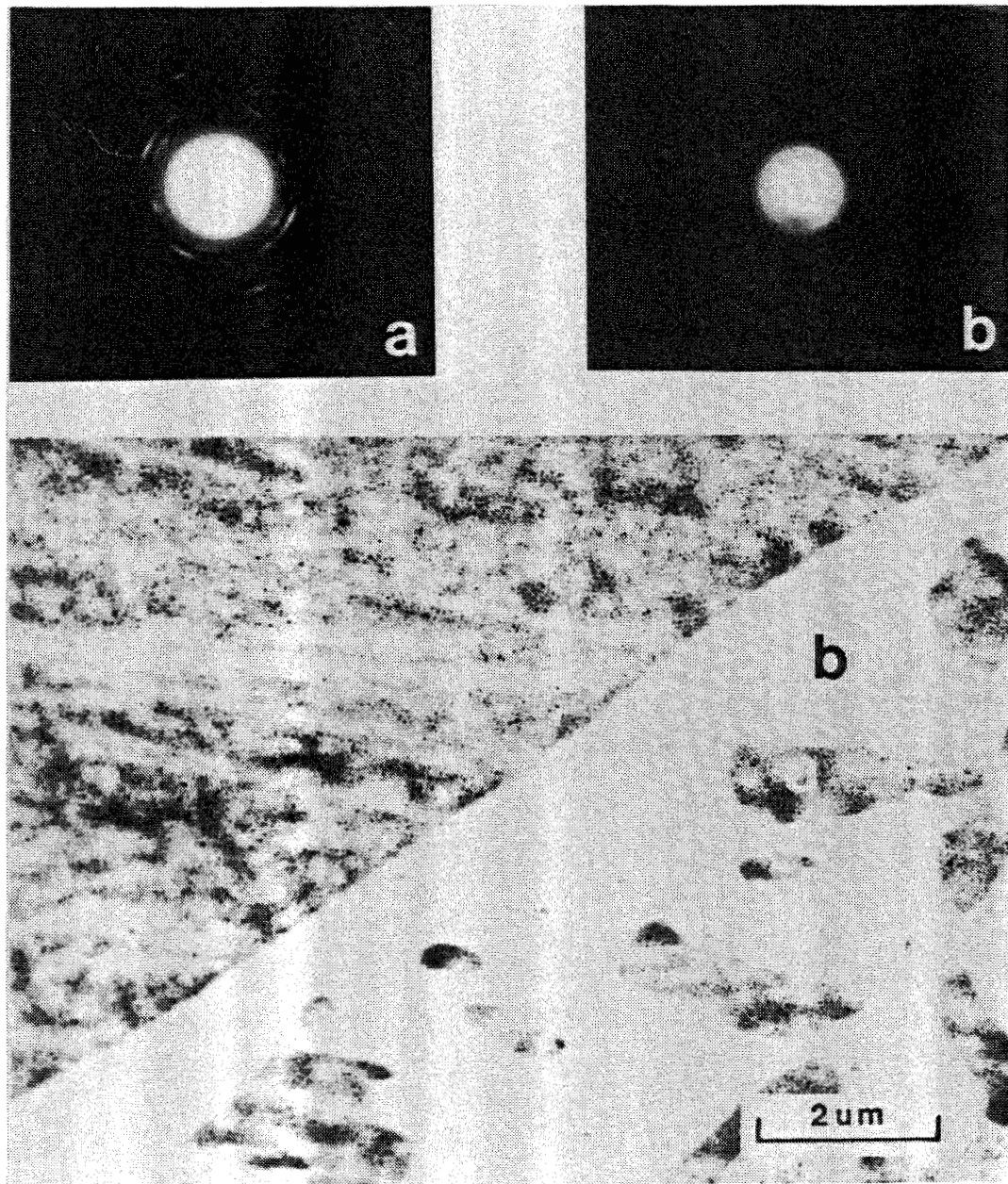


Figure 19: TEM micrograph of Ni-20Si oxidized in air at 950°C for an hour with selected area diffraction patterns from regions marked 'a' and 'b'.



Figure 20: Morphologies of Ni-20Si after 30 minutes of oxidation at 950°C in gas composition 'B'.

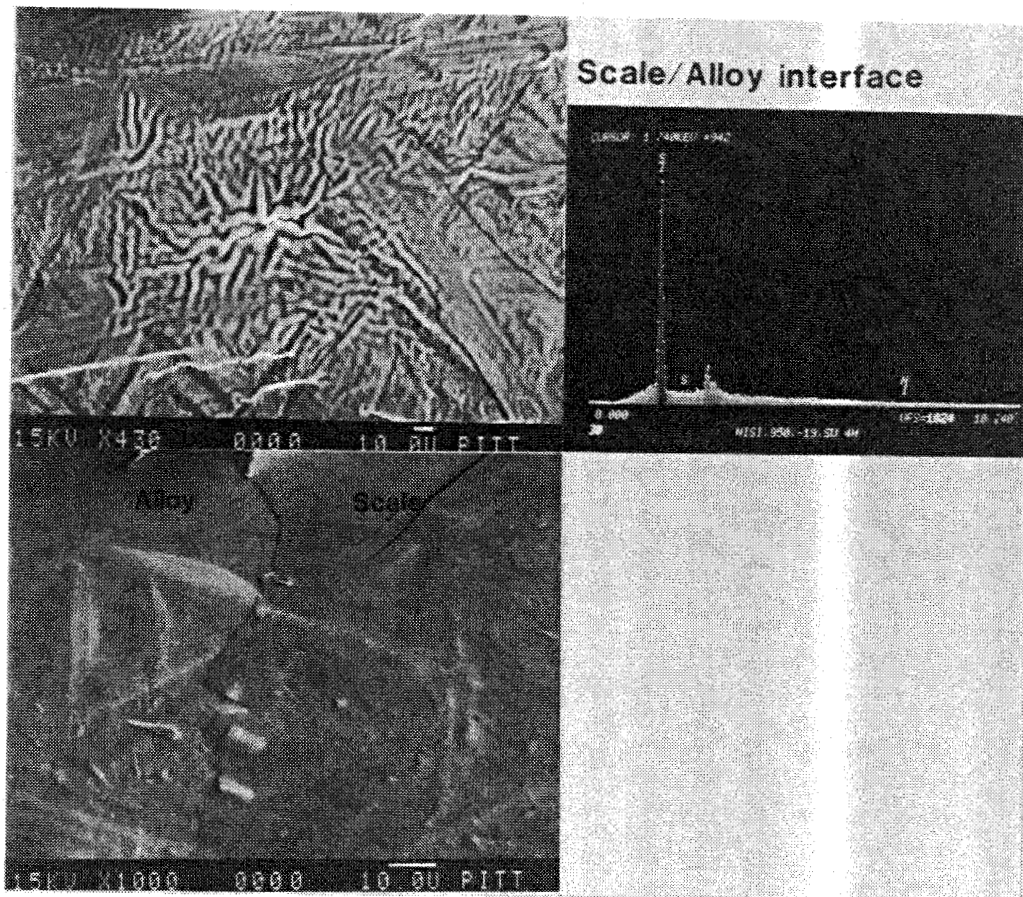


Figure 21: Ni-20Si exposed to gas composition 'B' for 30 minutes and subsequently exposed to gas composition 'E' for 4 hours at 950°C.

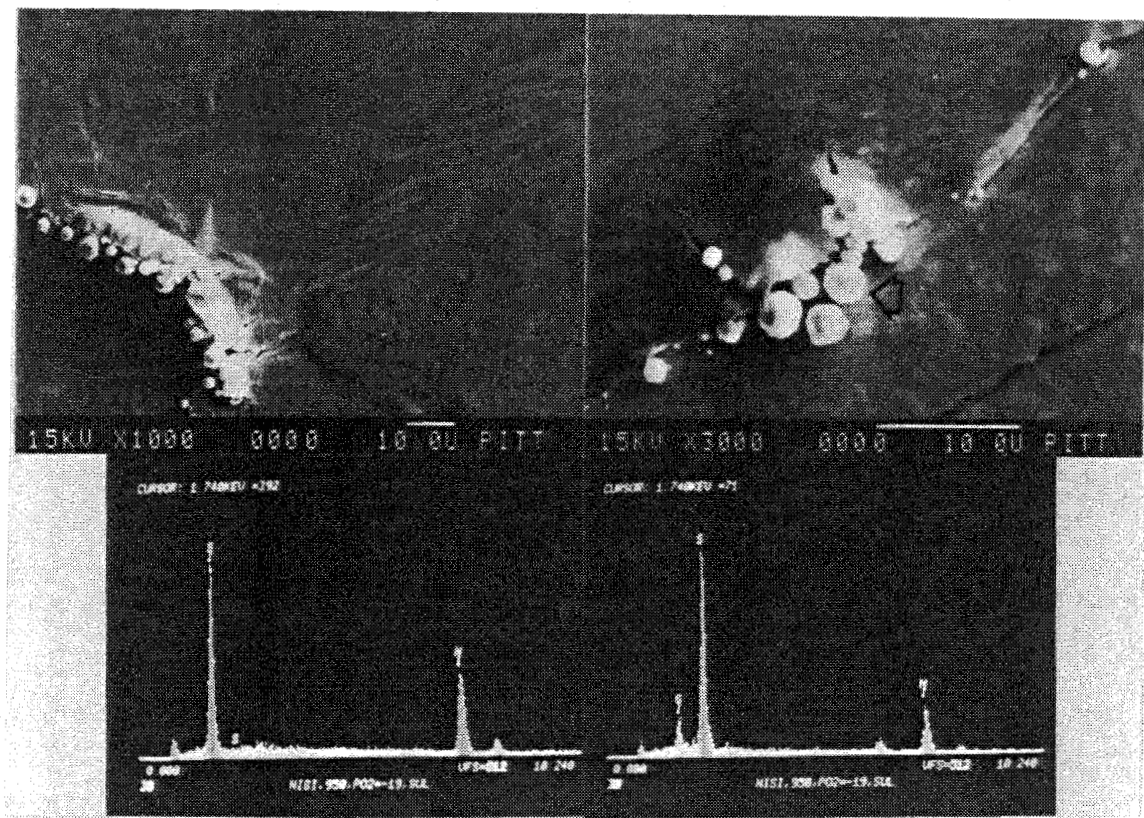


Figure 22: Ni-20Si exposed to gas composition 'B' for 30 minutes and subsequently exposed to gas composition 'E' for 4 hours at 950°C.

scale both after preoxidation and sulfidation/oxidation. When Ni-20Si was sulfidized in gas composition "A" after 24 hours of preoxidation in air, porosity was not observed at the scale surface. Thus preoxidation in a high oxygen potential can prevent the formation of the type of porosity in Ni-20Si shown in Figure 4.

DISCUSSION

Sulfidation

Sulfidation of Ni-20Si in H_2/H_2S mixtures (gas composition 'A') at $950^\circ C$ results in large amounts of porosity on the surface, consistent with the observed weight loss. One may assume that the sulfidation of Ni-20Si is associated with the vaporization of some volatile species. Figure 23 illustrates the thermochemical stability diagram for volatile species for Si-S at $950^\circ C$ (a). The sulfur potential applied was $P_{S_2} = 10^{-6.1}$ atm. The vapor pressure of SiS is extremely high at this sulfur potential, on the order of 0.1 atm for $a_{Si} = 1$. One can easily conclude that the development of porosity on the alloy surface was mainly due to the vaporization of SiS. Surprisingly, nickel sulfide, which is thermodynamically stable in gas composition 'A', was not observed and instead, the deep penetration of porosity into the alloy was observed. A SiO_2 layer, which has been confirmed by WDX and EDX analysis, forms on the surface even though porosity exists. For the study of sulfidation of Ni-20Si, trace amounts of oxygen-bearing impurities in the component gases may play an important role in the formation of the oxide scale. An oxygen partial pressure of about 10^{-26} atm at $950^\circ C$ has been estimated previously.¹⁴ This potential is high enough to form a SiO_2 layer.

As discussed in the section on oxidation behavior, Ni-20Si forms an extremely thin layer of vitreous SiO_2 on the surface. Furthermore, the initial formation rate of SiO_2 is fast probably due to the lower solubility of oxygen in Ni-Si. It is believed that initially a thin SiO_2 layer forms during the heat-up period of the

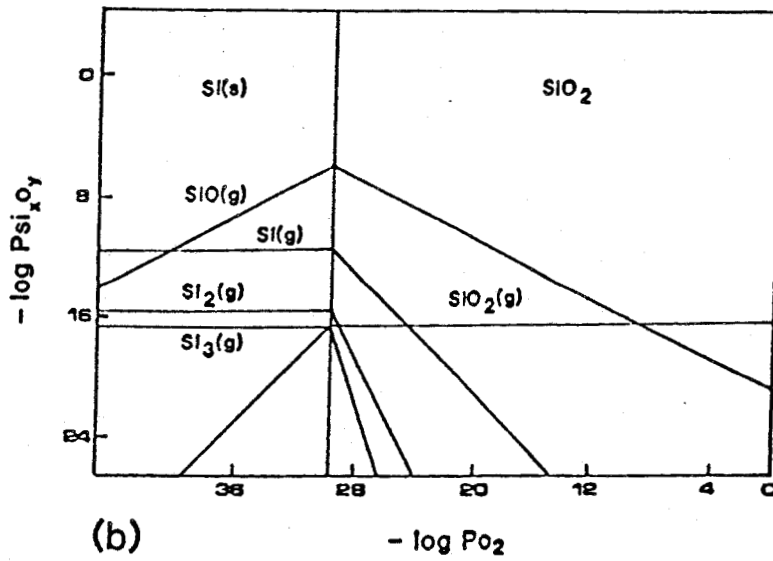
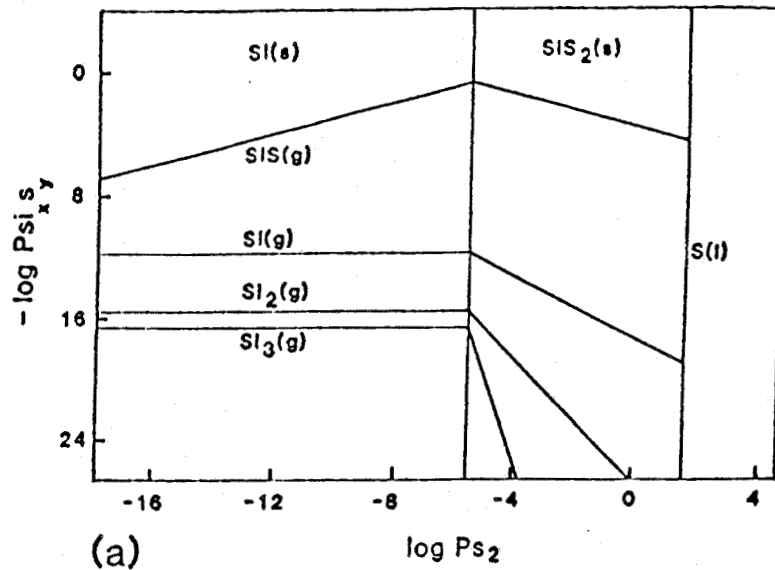
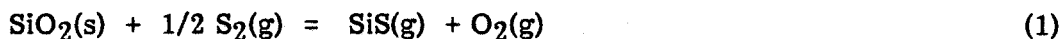


Figure 23: Stability diagrams for volatile species
 (a) Si-S and (b) Si-O at 950°C.

specimen, because at lower temperatures the vapor pressure of SiS is quite low (e.g., $P_{\text{SiS}} = 2.7 \times 10^{-3}$ atm at 700°C). Once a SiO_2 layer forms, the vaporization of SiS and SiO at the gas/ SiO_2 interface may occur by following reactions



$$K = P_{\text{SiS}} \times P_{\text{O}_2} / a_{\text{SiO}_2} \times (P_{\text{S}_2})^{1/2} \quad (2)$$

or



$$K = P_{\text{SiO}} \times (P_{\text{O}_2})^{1/2} / a_{\text{SiO}_2} \quad (4)$$

By assuming unit activity of SiO_2 in equations (2) and (4) and an oxygen partial pressure of about 10^{-26} atm resulting from trace amounts of oxygen-bearing impurities in the gases, calculated vapor pressures of SiS and SiO at 950°C were $P_{\text{SiS}} = 1.34 \times 10^{-5}$ atm and $P_{\text{SiO}} = 1.09 \times 10^{-8}$ atm. The formation of transient oxide (NiO) was also negligible. The preformed SiO_2 layer is unlikely to be permeable to sulfur and nickel thus the SiO_2 layer appears to be degraded mainly by the vaporization of SiS. The amounts of porosity in single phase (δ) is slightly more than that in two phase mixtures ($\delta + \text{Ni}_3\text{Si}_2$). However, the difference in amounts of porosity is not believed to be significant.

As the oxide scales are being thinned by the vaporization of SiS, the SiO_2 layers are apparently rehealed. The degradation of Ni-20Si by $\text{H}_2/\text{H}_2\text{S}$ mixtures (gas composition 'A') at 950°C is schematically illustrated in Figure 24.

Breakdown of Preformed Oxide Scales

Preformed Cr_2O_3 Scales

After 30 minutes of oxidation in an $\text{H}_2/\text{H}_2\text{O}$ mixture (gas composition 'B') at 950°C , $\alpha\text{-Cr}_2\text{O}_3$ forms on Ni-30Cr. The oxide layer is relatively smooth and shows no indication of cracking or spalling. However, a considerable number of voids are formed at the oxide scale/alloy interface, as shown in Figure 7. It has been

generally accepted that these voids are formed due to vacancy injection through the Cr_2O_3 scale,^{15,16} Kirkendall effects in the alloy^{17,18} and/or grain boundary sliding by a creep cavitation mechanism.^{3,19} For the Cr_2O_3 -forming alloys, new oxides form at the scale/gas interface because chromium diffuses much faster than oxygen through the oxide scale. The voids act as diffusion barriers for the transport of chromium from the alloy if the transport of chromium from the alloy by vaporization through the voids is not significant. In this case, the thickness of the oxide scale over the voids is less than that away from the voids. Chromium transport, both through the voids and across the scale/alloy interface, and the subsequent development of differential scale thickness are illustrated in Figure 25.

At any time during the oxidation period, the rate of evaporation of chromium from the alloy surface of the voids at a given temperature can be calculated from published chromium vapor pressures^{20,21} and the Langmuir equation

$$R_{\text{Cr}}(\text{alloy}) = a_{\text{Cr}} \times P \times (M/2\pi RT)^{1/2}, \text{ g/cm}^2.\text{sec} \quad (5)$$

where R_{Cr} is the rate of chromium vaporization from the alloy, a_{Cr} is the activity of chromium at the alloy surface, P is the vapor pressure of pure chromium, M is the atomic weight of chromium, R is the gas constant and T is absolute temperature.

Recently, Azhar²² developed computer models to calculate chromium concentration profiles in Ni-30Cr during oxidation at 950°C. By utilizing these results for the Cr concentration gradient in Ni-30Cr after 30 minutes of oxidation at 950°C, the flux of chromium to the scale/alloy interface can be calculated using Fick's first law.

$$J_{\text{Ni-30Cr}} = -D_{\text{Ni-30Cr}}^{\text{Cr}} \times (\Delta C/\Delta X), \text{ g/cm}^2.\text{sec} \quad (6)$$

where $J_{\text{Ni-30Cr}}$ is the flux of chromium, $D_{\text{Ni-30Cr}}^{\text{Cr}}$ is the diffusivity of chromium in Ni-30Cr, ΔC is the concentration difference and ΔX is the distance.

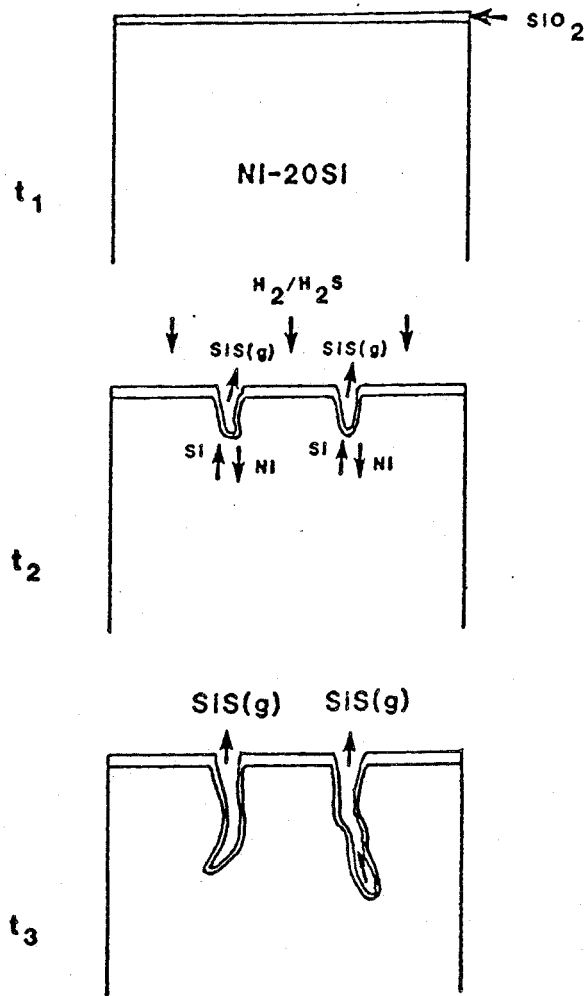


Figure 24: Schematic representation of degradation of Ni-20Si in gas composition 'A' at 950°C.

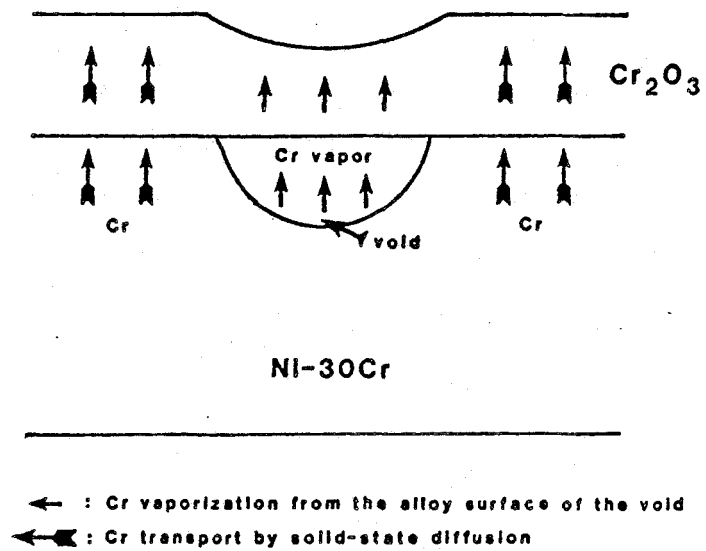


Figure 25: Schematic drawing of different oxide thickness due to the formation of a void at the scale/alloy interface.

The flux of Cr through the Cr_2O_3 scale after 30 minutes of oxidation at 950°C may also be expressed by²³

$$J_{\text{Cr}_2\text{O}_3} = - C_{\text{Cr}} \times (K_p/X), \text{ g/cm}^2.\text{sec} \quad (7)$$

where $J_{\text{Cr}_2\text{O}_3}$ is the flux of chromium through the Cr_2O_3 scale in $\text{g/cm}^2.\text{sec}$, C_{Cr} is the concentration of chromium in the oxide scale in g/cm^3 , K_p is the parabolic rate constant in cm^2/sec and X is the oxide scale thickness in cm.

Calculated values of the rate of chromium vaporization across the voids, the flux of chromium at the scale/alloy interface away from the voids and the flux of chromium through the oxide scale after 30 minutes of oxidation at 950°C are $5.7 \times 10^{-10} \text{ g/cm}^2.\text{sec}$, $4 \times 10^{-8} \text{ g/cm}^2.\text{sec}$ and $3.5 \times 10^{-8} \text{ g/cm}^2.\text{sec}$, respectively. The chromium flux at the scale/alloy interface away from the voids and the flux through the oxide scale are comparable and two orders of magnitude more than the rate of chromium vaporization across the voids at 950°C . These results are consistent with the thinner oxide scale over the voids, shown in Figure 7.

When voids are formed at the oxide/alloy interface, they may act as concentration sites for thermal stresses induced during cooling. This may lead to crack formation in and spalling of the oxide scale. Acoustic emission studies of the oxidation of Ni-30Cr at 950°C indicated that cracking and/or spalling of the Cr_2O_3 layer did not occur. A number of authors proposed gaseous transport through microchannels which were developed through the oxide scale by the so called 'dissociation mechanism'. However, the porous oxide, which is characteristic of the oxide formed by the dissociation mechanism, at the oxide scale/alloy interface was not observed after 30 minutes of oxidation at 950°C . Microchannels are unlikely to form through the oxide scale. Since the possibility of gas phase diffusion through cracks and/or spalling of the scale and microchannels of the oxide scale are ruled out, the protectiveness of the scale appears to solely depend on the

solid-state diffusion of reactive species. In other words, if degradation occurs by the diffusion of reactive species, such as sulfur or metallic elements, through the preformed oxide scale, the differential scale thickness may play an important role in the degradation of the scale.

Breakdown of Preformed Cr_2O_3 Scales

Upon exposure of the preoxidized Ni-30Cr alloy to sulfur-bearing gases, sulfur penetrates the preformed Cr_2O_3 layer because the effective diffusivity of sulfur through Cr_2O_3 is about two orders of magnitude greater than the diffusivity of chromium through the oxide scale.^{24,25} It takes less time for sulfur to penetrate through the oxide scale over the voids, whose thickness is less than that away from the voids. Consequently, sulfur arrives at the scale/void interface and moves to the rim of the voids, probably by surface diffusion. The chromium activity at the rim of the voids is high because chromium evaporation is negligible at 950°C. Internal sulfides, mainly chromium sulfides, nucleate at the triple point of the scale, the void and the alloy substrate. Figure 26 shows the concentration profile of sulfur in Ni-30Cr which was oxidized in gas composition 'B' for 30 minutes and subsequently exposed to gas composition 'E' for 4 hours at 700°C. The formation of external sulfides is predominant where voids exist, as shown in (a) of Figure 26. A line scan of sulfur in (b) of Figure 26 shows the sharp increase of sulfur concentration at the rim of the voids. This suggests that sulfur is concentrated at the rim of the voids prior to the formation of external sulfide. In other words, sulfur penetrates preferentially through Cr_2O_3 over the voids and moves to the rim of the voids, where internal sulfides form. This result is consistent with the formation of ring-shape internal sulfides, which were observed on the underside of the Cr_2O_3 layer, shown in Figure 11. Sulfide nucleation and subsequent growth in the voids are not restricted by a retarding substrate. Internal

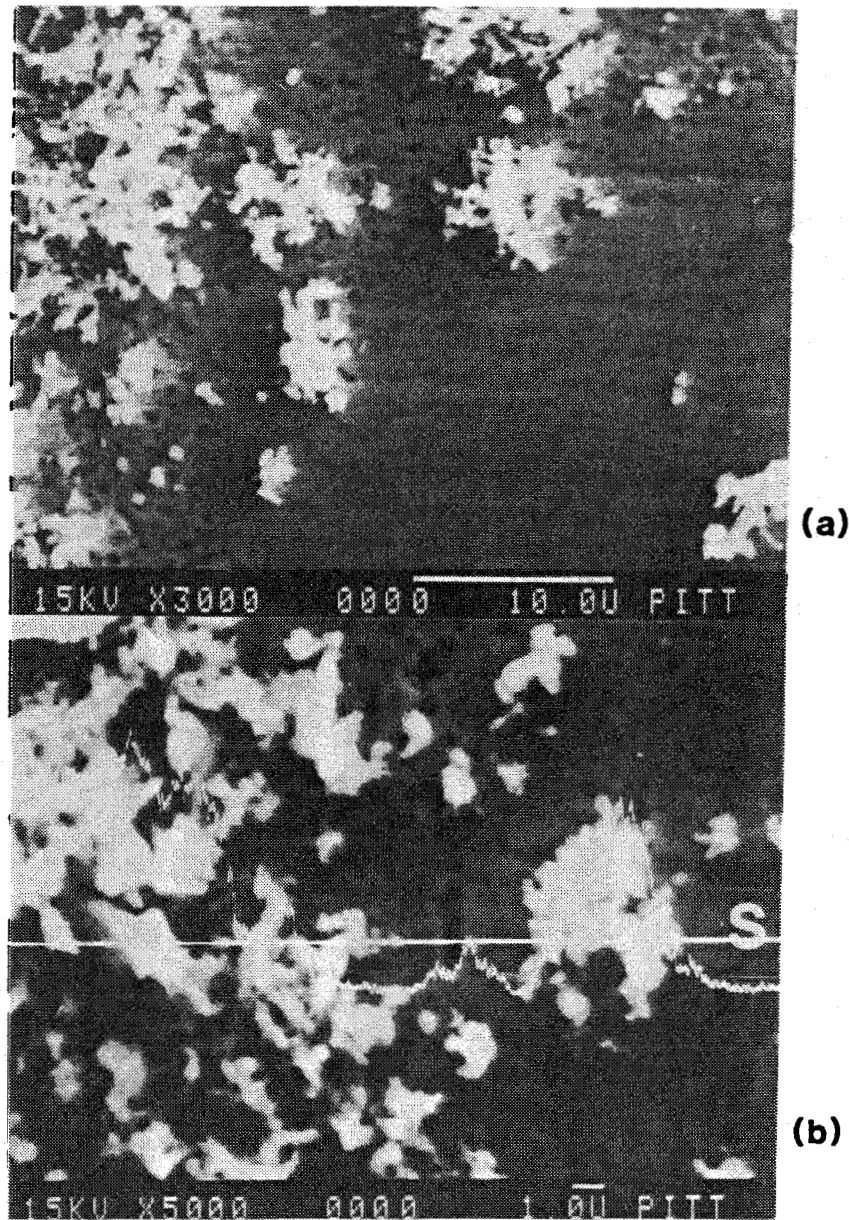
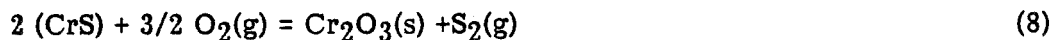


Figure 26: Concentration profile of sulfur on Ni-30Cr which was oxidized in gas composition 'B' for 30 minutes and subsequently exposed to gas composition 'E' for 4 hours at 700°C.

sulfides grow from the underside of the scale in the voids and progressively fill the voids by the inward diffusion of sulfur. At the same time, outward moving chromium through chromium sulfides and inward moving sulfur through the Cr_2O_3 scale react at the oxide/sulfide interface and progressively form sulfide-rich channels, which are easy paths for metal transport, because the chromium diffusion through sulfide is several orders of magnitude faster than that through chromium oxide.²⁶ As the internal sulfides fill the voids at the scale/alloy interface, newly formed sulfides in the voids and sulfide rich channels through the oxide scale enhance mainly chromium transport. Consequently, chromium reaches the scale/gas interface and reacts with sulfur from the gas phase. Chromium sulfide is not thermodynamically stable at the scale/gas interface. However, nickel also diffuses out through the sulfide-rich channels and results in a gradual decrease in the activity of chromium at the scale/gas interface, accompanied by an increase in the activity of nickel. Eventually the activity of chromium at the scale/gas interface approaches values for which alloyed chromium sulfide is stable and the Cr_2O_3 scale stops growing, whereas the alloyed chromium sulfide begins to grow upon it.^{22,27} A thin layer of Cr_2O_3 may form on the alloyed chromium sulfide by reaction (8).



where (CrS) indicates CrS dissolved in NiS-CrS solution. As the activity of chromium in the sulfide increases in the early stage of sulfidation/oxidation, Cr_2O_3 can form on the alloyed chromium sulfide. This oxide layer was observed in the early stages of degradation. As the sulfidation/oxidation continues, nickel diffuses out through the sulfide-rich channels to form virtually pure nickel sulfides on top of the alloyed chromium sulfide. The formation of nickel sulfides, which are thermodynamically stable at the scale/gas interface, accelerates the degradation

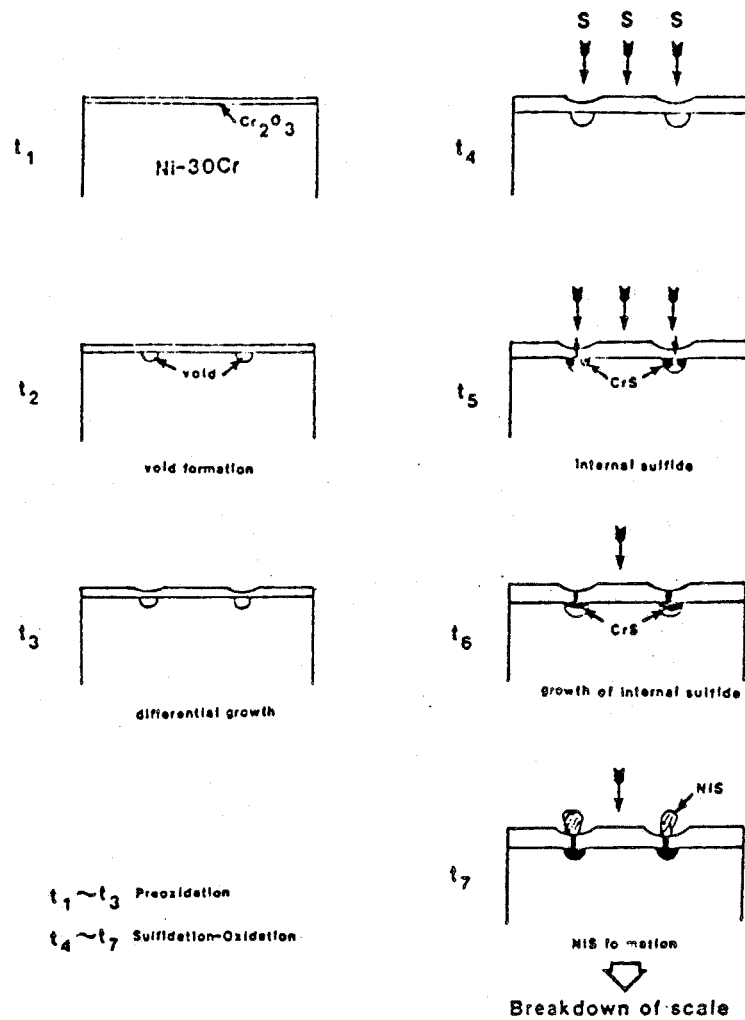


Figure 27: Schematic representation of the breakdown of preformed Cr_2O_3 scale formed on Ni-30Cr by sulfur-bearing gases.

processes because these sulfides are liquid at 950°C and breakdown of the oxide scale occurs. The proposed mechanism of breakdown of preformed Cr₂O₃ on Ni-30Cr by sulfur-bearing gases is schematically illustrated in Figure 27. This mechanism may not apply to the Fe-Cr system because the diffusivity of Fe through Cr₂O₃ is higher and the Cr₂O₃ layer formed on Fe-Cr is less pure. The protectiveness of preformed Cr₂O₃ scales on Ni-30Cr against sulfur-bearing gases was improved by high temperature preoxidation, such as 1150°C, as shown in Table 2. Preoxidation at higher temperature provides a more protective Cr₂O₃ layer mainly due to increased scale thickness. Even though larger voids are formed at the scale/alloy interface, the thickness of the oxide scale over the voids is comparable to that away from the voids because transport of chromium vapor through the voids becomes comparable to the flux of chromium through the oxide scale at the higher temperature

Preformed Al₂O₃ Scales

When Fe-18Cr-6Al is oxidized at 950°C in a H₂/H₂O mixture for 30 minutes, a γ-Al₂O₃ layer forms on the alloy surface. This oxide scale suffers large amounts of cracking during cooling. Acoustic emission studies on the oxidation of Fe-18Cr-6Al at 950°C in air indicated isothermal cracking was insignificant compared to cracking during cooling. Therefore, the large amounts of cracking and spalling, shown in Figure 12, occur during cooling, but some isothermal cracking was observed, particularly with wet air. A considerable number of voids, exist at the scale/alloy interface, as shown in Figure 12. The addition of hafnium to Fe-18Cr-6Al provides a smooth crack-free γ-Al₂O₃ scale on the alloy surface. Generally the scale/alloy interface of Fe-18Cr-6Al-1Hf was smooth and did not include the voids, observed in Ni-30Cr and Fe-18Cr-6Al. However, the hafnium oxide pegs, formed during the oxidation, are believed to attract all the vacancies at the

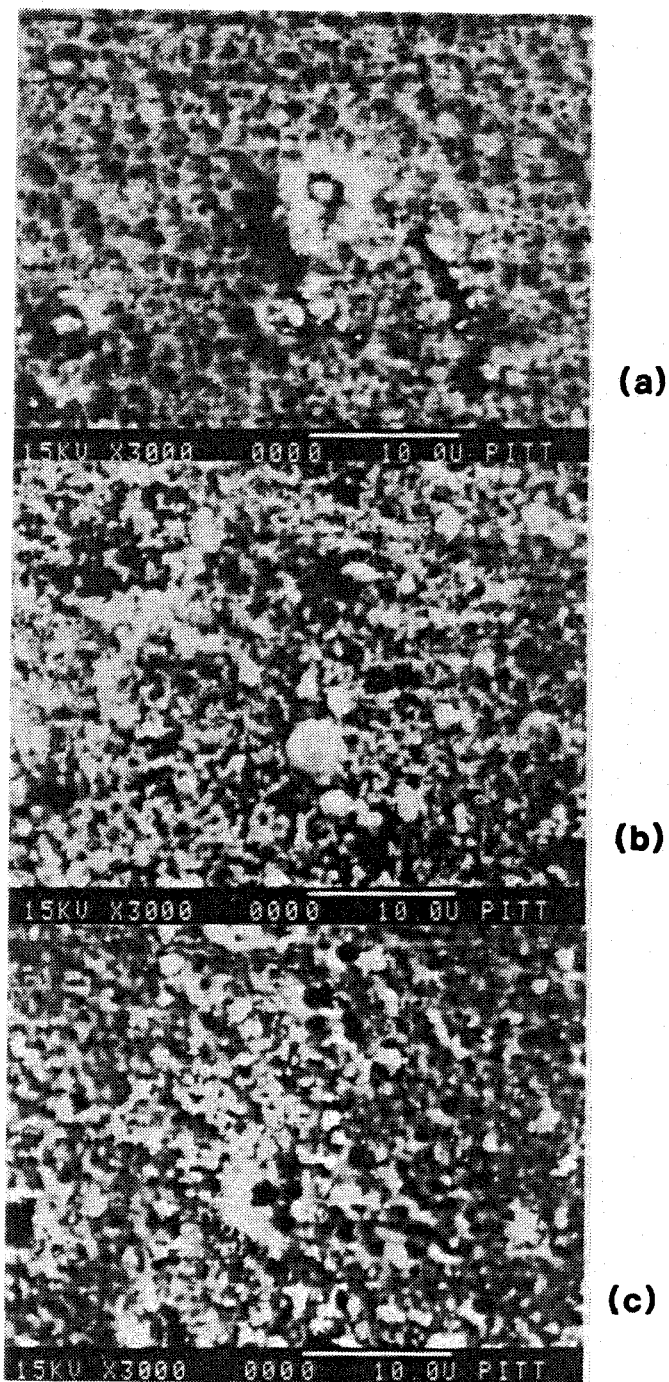


Figure 28: Morphologies of (a) the external scale surface, (b) the underside of the scale and (c) the alloy substrate of Fe-18Cr-6Al-1Hf after 30 minutes of oxidation in gas composition 'B' at 1150°C.

scale/alloy interface, resulting in the formation of craters around the HfO_2 .^{28,29} The overall scale adherence was improved by the addition of hafnium. However, the formation of HfO_2 gave rise to the formation of the craters in the alloy substrate, shown in Figure 13, which are not favorable for scale integrity. Higher preoxidation temperature produced more HfO_2 protrusions with a larger volume of voids surrounding them, as shown in Figure 28.

Breakdown of Preformed Al_2O_3 Scales

When the preoxidized Fe-18Cr-6Al alloy was exposed to sulfur-bearing gases at 950°C , the number of sulfides at the scale/gas interface was fewer than that on Fe-18Cr-6Al-1Hf but the size of the sulfides was significantly larger. The Al_2O_3 scale adherence on Fe-18Cr-6Al was observed to be very poor, as shown in Figure 18. Huang, et al.³⁰ reported the cracking of oxide scales formed on Fe-Cr-Al in a $\text{H}_2/\text{H}_2\text{S}/\text{H}_2\text{O}$ gas mixture at 900°C . Considering the isothermal cracking of the scale observed in acoustic emission studies, the formation of large sulfides is believed to be due to scale cracking.

The addition of 1 % hafnium to Fe-18Cr-6Al improved the oxide scale adherence and integrity and improved the sulfidation resistance. However, sulfide formation on Fe-18Cr-6Al-1Hf is always associated with the Hf-rich regions. When the preoxidized Fe-18Cr-6Al-1Hf alloy was exposed to the sulfur-bearing gases at 950°C , small iron sulfides form initially around HfO_2 in the Al_2O_3 scale because metallic iron is available on the external scale from the preoxidation stage. Metallic iron is especially rich around HfO_2 because hafnium exists as intermetallic compounds (HfFe_2) in the alloy and the oxidation of Hf to HfO_2 increases the localized iron concentration. This metallic iron reacts with sulfur at the scale/gas interface.

The presence of an oxygen active element (Y) on the sulfidation of Ni-Al and Ni-Cr alloys has been reported to promote the formation of Cr_2S_3 and Al_2S_3 .³¹ Deleterious effects of yttrium on the sulfidation-oxidation of Cr_2O_3 and Al_2O_3 forming alloys have been reported due to the build-up of growth stresses around yttrium rich regions and/or the thinner scale associated with such regions.^{3,7}

Hafnium has a fairly high affinity for sulfur. However, no published thermodynamic data for hafnium sulfide are available at this moment. Hafnium sulfides were estimated to be stable in gas composition 'E' at 950°C.³² In the present study, hafnium-rich sulfides were observed at the scale/alloy interface, shown in (b) of Figure 15. Apparently, the development of hafnium-rich sulfides through the oxide scale provides easier diffusion paths both for sulfur and for metallic components. Penetration of sulfur through the sulfides leads to the formation of internal hafnium-rich sulfides to fill the craters which were formed during preoxidation. Outward transport of chromium and iron through the hafnium-rich sulfides results in the formation of chromium and iron sulfides on the external oxide surface.

Furthermore, since the oxidation of hafnium increases the volume by 40 %, growth stresses may be accumulated in the hafnium oxide pegs during the preoxidation, but these stresses are not high enough to induce cracking or spalling during preoxidation. Upon sulfidation-oxidation, more growth stresses are expected to accumulate around the hafnium rich regions, leading to spalling of the scale, as shown in Figure 17.

The deleterious effect of hafnium on the sulfidation-oxidation of Fe-18Cr-6Al-1Hf has been confirmed by higher temperature preoxidation. As discussed before, with preoxidation at higher temperature, the sulfidation attack was worse, as shown in table 2. The examination of the preoxidized Fe-18Cr-6Al-1Hf revealed

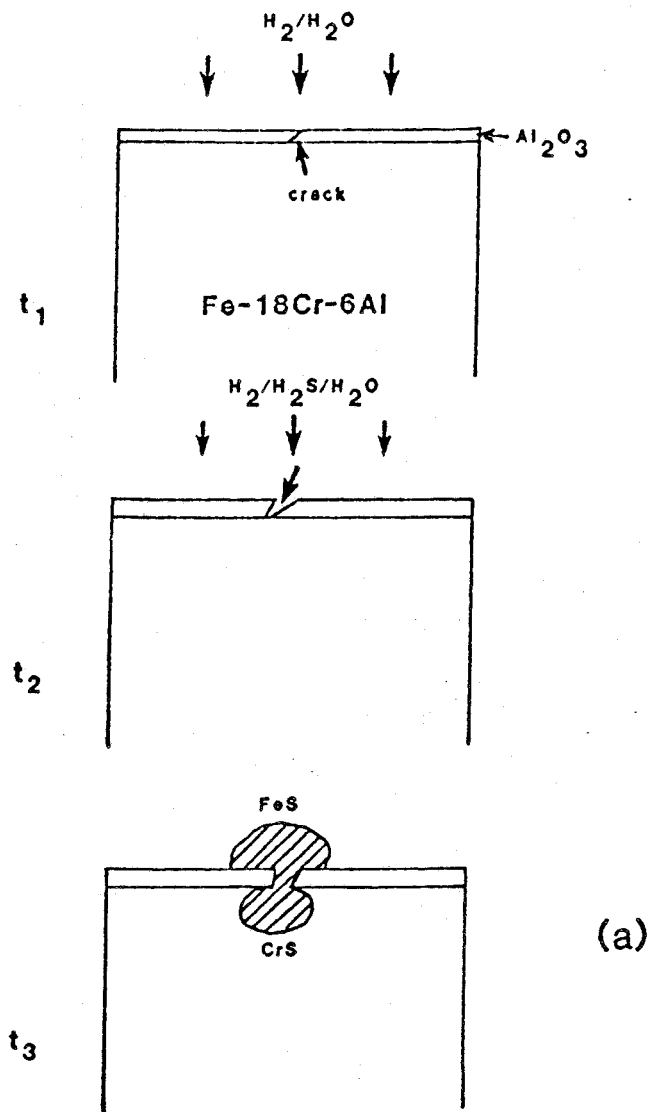
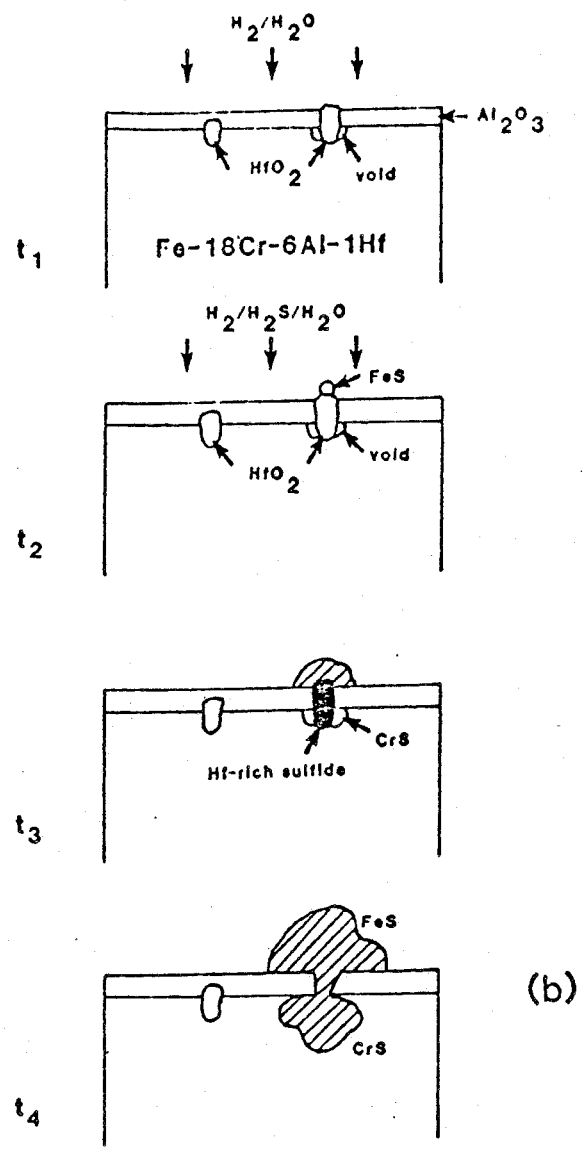


Figure 29: Schematic representation of the breakdown of preformed Al_2O_3 scale formed on (a) Fe-18Cr-6Al and (b) Fe-18Cr-6Al-1Hf by sulfur-bearing gases.



more hafnium oxides in the Al_2O_3 scale and voids at the scale/alloy interface. Acoustic emission tests were employed to check for cracking or spalling of the oxide scale during cooling to the sulfidation-oxidation temperature (950°C) from the preoxidation temperature (1150°C). The results showed negligible cracking and/or spalling in the scale.

It is proposed that the major part of the sulfidation attack may be attributed to the transformation of HfO_2 pegs to hafnium-rich sulfides, which are easy paths for diffusion of sulfur and metallic components through the Al_2O_3 scale and, secondly, the void formation around HfO_2 pegs in the alloy substrate. The proposed mechanism of breakdown of preformed Al_2O_3 scale by sulfur-bearing gases is schematically illustrated in Figure 29. Thus, while addition of Hf improves the overall resistance of Fe-Cr-Al to sulfidation/oxidation corrosion by improving the mechanical integrity of the scale, it provides easy transport paths through the scale for sulfur. Therefore, the use of an oxygen active element which does not produce 'pegs' may well be preferable to Hf.

Preformed SiO_2 Scales

Porosity was observed when Ni-20Si was oxidized in a low oxygen potential gas, as shown in Figure 20. The vapor pressure of SiO is high under these conditions, as indicated in (b) of Figure 23, and the formation of pores in the external SiO_2 scale is concluded to result from the evaporation of SiO. The porosity formation in the SiO_2 layer was prevented when this alloy was oxidized in air (high oxygen potential). This confirms the evaporation of SiO at low oxygen potentials. However, its effect on the degradation resistance does not appear to be significant.

Breakdown of Preformed SiO_2 Scales

When Ni-20Si was exposed to the sulfur-bearing gases, no apparent sulfidation attack was observed. The appearance of the specimens was quite similar to that of the preoxidized specimens. Porosity was observed in the external scale but the size of pores was negligible. This is attributed to the formation of a very thin layer of vitreous silica because of relatively low vapor pressures of SiS and SiO at 950°C in gas composition 'E' and extremely slow diffusion of sulfur and nickel through the vitreous SiO_2 layer. Importantly, voids at the scale/alloy interface do not exist even after sulfidation-oxidation.

When there are cracks in the brittle alloy, nickel sulfide nodules exist along the cracks. The formation of sulfide nodules can be explained as follows; since the crack is very narrow at the tip, the local oxygen potential in the gas phase equals the local oxygen potential in the thin layer of oxide along the crack. In this case sulfide formation is possible if the local oxygen potential is too low to form an oxide layer and the local sulfur potential is high enough to form nickel sulfide, which is liquid at the reaction temperature. In $\text{H}_2/\text{H}_2\text{S}/\text{H}_2\text{O}$ gas mixtures, $P_{\text{H}_2\text{S}}$ in cracks or pores in a preformed oxide layer is approximately constant.³³ Local depletion of oxygen at the tip of the crack and the high sulfur potential of gas composition 'E' lead to sulfide formation. These liquid sulfides move to the alloy surface, probably by capillarity. The proposed mechanism of the breakdown of preformed SiO_2 by sulfur-bearing gases is schematically illustrated in Figure 30.

With preformation of a SiO_2 layer at a high oxygen potential (such as air), no degradation was detected. The high vapor pressures of SiS and SiO are important considerations. However, the formation of a thin layer of vitreous silica and good scale adherence give resistance to sulfur penetration which is considerably greater than that for Cr_2O_3 or Al_2O_3 . It should be mentioned here that the excellent

plasticity of the SiO_2 scale without cracking at high temperatures provides the basis for practical applications, such as coatings.

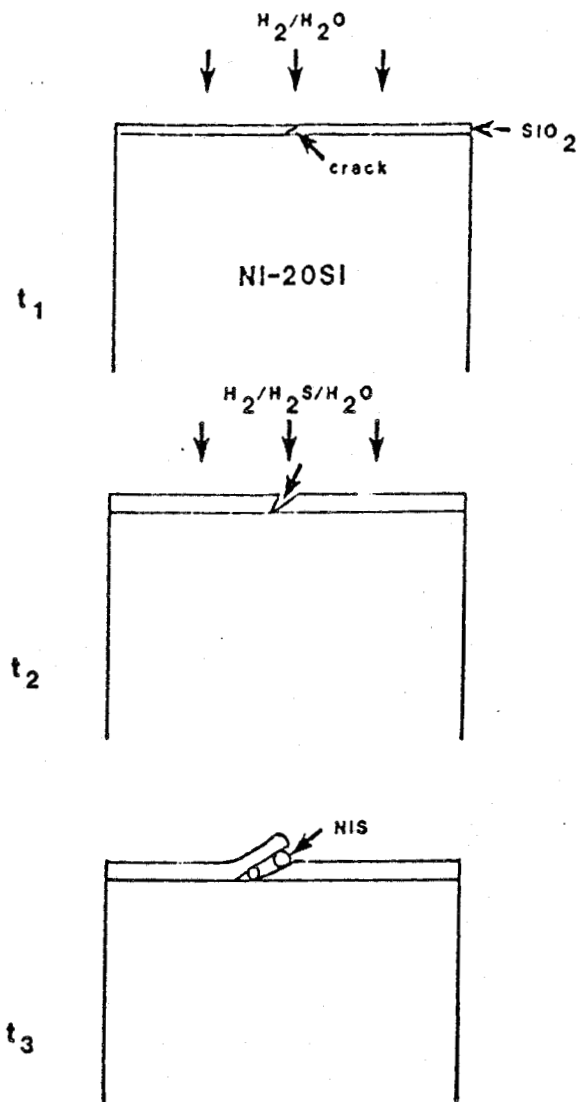


Figure 30: Schematic representation of the breakdown of preformed SiO_2 scale formed on Ni-20Si by sulfur-bearing gases.

CONCLUSIONS

 Cr_2O_3 Former (Ni-30Cr)

1. A Cr_2O_3 layer forms on the alloy surface during preoxidation. At the same time, voids form at the scale/alloy interface and act as barriers to chromium diffusion to the oxide scale because Cr vaporization at 950°C is slow. Consequently, these lead to the formation of a thinner oxide layer over the voids than that away from the voids.
2. Upon exposure to sulfur bearing gases, sulfur ions penetrate preferentially through the thin oxide scale over the voids and react with Cr ions to form internal sulfides at the rims of the voids where the chromium activity is high. As the sulfidation/oxidation continues, internal sulfides fill the voids and, at the same time, progressive formation of sulfides at the sulfide/oxide interface by the reaction between outward moving Cr ions and inward moving sulfur ions provides a sulfide rich channel through the scale, which is an easy path for Cr and Ni ion transport. This enables chromium sulfides and, then, nickel sulfides to form at the scale/gas interface, leading to scale breakdown.

 Al_2O_3 Former (Fe-18Cr-6Al-1Hf)

3. An Al_2O_3 layer with a distribution of HfO_2 particles forms on the alloy surface. During oxidation the hafnium oxides act as vacancy sinks and, subsequently, are surrounded by craters at the scale/alloy interface.
4. Upon exposure to sulfur bearing gases, sulfur reacts with metallic Fe, on the scale, and HfO_2 , through the Al_2O_3 layer, to form iron sulfides and HfS_2 , respectively. The formation of hafnium sulfide channels through the Al_2O_3 scale enhances inward transport of sulfur ions and outward transport of iron and chromium ions. Internal sulfides form in the craters in the scale/alloy interface and iron and chromium sulfides form at the scale/gas interface. It is concluded that Hf increases the oxidation resistance, but initiates the sulfidation attack.

 SiO_2 Former (Ni-20Si)

5. The sulfidation in $\text{H}_2/\text{H}_2\text{S}$ at 950°C produces porosity in the alloy due to the high vapor pressure of SiS. However a thin layer of vitreous SiO_2 is still effective in preventing the voluminous formation of nickel sulfides.
6. A thin layer of vitreous silica forms on the alloy surface during preoxidation. Good contact between the oxide scale and substrate was also obtained. Upon exposure to sulfur bearing gases, no apparent attack was observed. This can be explained by the formation of a vitreous silica layer with good scale adherence on the alloy surface providing good protection from sulfur penetration unless there is a crack in the alloy.

REFERENCES

1. K. Natesan, "High Temperature Corrosion in Coal Gasification Systems", Corrosion, Vol. 18, 1985, pp. 646.
2. R. A. Perkins and S. J. Vonk, "Corrosion Chemistry in Low Oxygen Activity Atmospheres", Tech. report 979-6. Lockheed Palo Alto Research Laboratory, December 1979.
3. F. H. Stott and M. F. Chong, "The Influence of Preoxidation on the Degradation of Alloys in Sulfur-Containing Gases at High Temperature", Corrosion resistant Materials for Coal Conversion Systems, D. B. Meadowcroft and M. I. Manning, ed., Applied Science Publishers, London and New York, 1983, pp. 491.
4. G. J. Yurek, M. H. LaBranche and Y. K. Kim, "Oxidation of Cr and Fe-25Cr Alloy in H₂-H₂O-H₂S Gas Mixtures at 900°C", High Temperature Corrosion in Energy Systems", M. F. Rothman, ed., AIME", 1985, pp. 295.
5. D. Bruce and P. Hancock, "Influence of Mechanical Properties of Surface Oxide Films on Oxidation Mechanism", Journal of Institute of Metals, Vol. 97, 1969, pp. 140, 148.
6. A. Rahmel", "Kinetic Conditions for the Simultaneous Formation of Oxide and Sulfide in Reaction of Iron with Gases Containing Sulfur and Oxygen or Their Compounds", Corrosion Science", Vol. 13, 1973, pp. 125.
7. F. H. Stott, F. M. Chong and C. A. Stirling, "Preoxidation for Protection of High Temperature Alloys in Environments of High Sulfur and Low Oxygen Potentials pertinent to Gasification Processes", High Temperature Corrosion in Energy Systems", M. F. Rothman, ed., AIME, 1985, pp. 253.
8. M. H. LaBranche, A. Garratt-Reed and G. J. Yurek, "Early Stages of the Oxidation of Chromium in H₂/H₂O/H₂S Gas Mixtures", Journal of Electrochemical Society, Vol. 130, 1983, pp. 2405.
9. P. A. Mari, J. M. Chaix and J. P. Larpin, "Protection of Fe-Cr-Al Alloys in Sulfidizing Environments by Means of Al₂O₃ Scale", Oxidation of Metals, Vol. 17, 1982, pp. 315.
10. T. T. Huang, B. Peterson, D. A. Shores and E. Pfender, "XPS and AES studies of High Temperature Corrosion Mechanism of Fe-30Cr Alloys", Corrosion Science, Vol. 24, 1984, pp. 167.
11. G. H. Meier and E. A. Gulbransen, "Thermochemical Stability Diagrams for Condensed Phases and Volatility Diagrams of Volatile Species over Condensed Phases in Twenty Metal-Sulfur-Oxygen Systems between 1150 - 1450°K", DOE Report on Contract No DE-AC-01-79-ET-13547, 1980.

12. O. Kubaschewski and C. B. Alcock, "Metallurgical Thermochemistry", Pergamon Press, New York, 1979.
13. A. A. Ashary, G. H. Meier and F. S. Pettit, "Acoustic Emission of Oxide Cracking During Alloy Oxidation", High Temperature Protective Coatings", S. C. Singhal, ed., AIME, 1983.
14. G. M. Kim, The Breakdown of Preformed Oxide Scales on Ni-30Cr, Fe-18Cr-6Al-1Hf and Ni-20Si in Sulfur and Carbon-Bearing Gases, Ph.D. dissertation, University of Pittsburgh, 1986.
15. R. H. Hales and A. C. Hill, "The Role of Metal Lattice Vacancies in the High Temperature Oxidation of Nickel", Corrosion Science, Vol. 12, 1972, pp. 843.
16. V. R. Howes, "Metal-Oxide Interface Morphology for a Range of Fe-Cr Alloys", Corrosion Science, Vol. 10, 1970, pp. 99.
17. J. D. Kuenzly and D. L. Douglass, "The Oxidation Mechanism of Ni₃Al Containing Yttrium", Oxidation of Metals, Vol. 8, 1974, pp. 139.
18. C. S. Giggins and F. S. Pettit, "The Oxidation of TD NiC (Ni-20Cr-2vol pct ThO₂) between 900°C - 1200°C", Metallurgical Transactions, Vol. 2, 1971, pp. 1071.
19. M. J. Graham and D. J. Caplan, "Detection of CO₂ in Cavities in NiO Scale", Journal of Electrochemical Society, Vol. 120, 1973, pp. 769.
20. E. A. Gulbransen and K. F. Andrew, "Vapor Pressure studies on Iron and Chromium and Several Alloys of Iron, Chromium and Aluminum", Transactions of the Metallurgical Society of AIME", Vol. 221, 1961, pp. 1247.
21. O. Kubaschewski and G. Heyer, "The Thermodynamics of the Chromium-Iron systems", Acta Metallurgica, Vol. 8, 1960, pp. 416.
22. T. Azhar, "Thermodynamic and Kinetic Analysis of Ni-Cr-O-S, Ni-Al-O-S and Ni-Si-O-S Systems", Masters Thesis, University of Pittsburgh", 1986.
23. N. Birks and G. H. Meier, "Introduction to High Temperature Oxidation of Metals", Edward Arnold, ed., London, 1983.
24. H. Hindam and D. P. Whittle, "Microstructure, Adhesion and Growth Kinetics of Protective Scales on Metals and Alloys", Oxidation of Metals, Vol. 18, 1982, pp. 245.
25. K. N. Strafford and P. J. Hunt, "The Mechanism of Transport of Sulfur across Scales and the Corrosion of Materials in Bi-oxidant Oxygen-Sulfur Environments", High Temperature Corrosion, R. A. Rapp, ed., NACE, San Diego, 1981, pp. 380.
26. S. Mrowec and K. Przybylski, "Transport Properties of Sulfide Scales and sulfidation of Metals and Alloys", Oxidation of Metals, Vol. 23, 1985, pp. 107.

27. C. S. Giggins and F. S. Pettit, "Corrosion of Metals and Alloys in Mixed Gas Environments at Elevated temperatures", *Oxidation of Metals*, Vol. 14, 1980, pp. 363.
28. J. K. Tien and F. S. Pettit, "Mechanism of Oxide Adherence on Fe-25Cr-4Al (Y or Sc) Alloys", *Metallurgical Transactions*, Vol. 3, 1972, pp. 1587.
29. D. P. Whittle and J. Stringer, "Improvements in High Temperature oxidation Resistance by Additions of Reactive Elements or Oxide Dispersions", *Philosophical transaction of Royal Society*, Vol. A295, 1980, pp. 309.
30. T. T. Huang, Y. C. Lin, D. A. Shores and E. Pfender, "Corrosion of FeCrAl, FeCrAlY and FeCrAlHf Alloys in High Temperature H₂-H₂S-H₂O Environment", *Journal of Electrochemical Society*, Vol. 131, 1984, pp. 2191.
31. E. J. Vinverg and D. L. Douglass, "The Sulfidation Behavior of Nickel-Chromium and Nickel-Aluminum bearing Alloys with and without Yttrium", *High Temperature Corrosion Transactions*, Japan Institute of Metals, 1983, pp. 507.
32. G. H. Meier, Unpublished data.
33. G. J. Yurek and M. H. LaBranche, "Oxidation of Chromium in H₂/H₂O/H₂S Gas Mixture", *Corrosion-Erosion-Wear of Materials in Emerging Fossil Energy Systems*, A. V. Levy, ed., NACE, Berkeley, California, 1982, pp. 933